

Review

Morphological Investigation of Protein Crystals by Atomic Force Microscopy

Silvia Maria Cristina Rotondi ¹, Giorgia Ailuno ², Simone Luca Mattioli ³, Alessandra Pesce ^{1,*}, Ornella Cavalleri ^{1,*} and Paolo Canepa ¹

¹ Department of Physics, University of Genova, Via Dodecaneso 33, 16146 Genova, Italy; silviamariacristina.rotondi@edu.unige.it (S.M.C.R.); paolocanepa@unige.it (P.C.)

² Department of Pharmacy, University of Genova, 16148 Genova, Italy; giorgia.ailuno@unige.it

³ Research & Early Development, Dompè Farmaceutici S.p.A., Via De Amicis 95, 80131 Napoli, Italy; simone.mattioli@dompe.com

* Correspondence: pesce@fisica.unige.it (A.P.); ornella.cavalleri@unige.it (O.C.)

Abstract: In this review, we discuss the progress in the investigation of macromolecular crystals obtained through the use of atomic force microscopy (AFM), a powerful tool for imaging surfaces and specimens at high resolution. AFM enables the visualization of soft samples at the nanoscale and can provide precise visual details over a wide size range, from the molecular level up to hundreds of micrometers. The nonperturbative nature, the ability to scan in a liquid environment, and the lack of need for freezing, fixing, or staining make AFM a well-suited tool for studying fragile samples such as macromolecular crystals. Starting from the first morphological investigations revealing the surface morphology of protein crystals, this review discusses the achievements of AFM in understanding the crystal growth processes, both at the micro- and nanoscale. The capability of AFM to investigate the sample structure at the single molecular level is analyzed considering in-depth the structure of S-layers. Lastly, high-speed atomic force microscopy (HS-AFM) is discussed as the evolution to overcome the limitations of low imaging speed, allowing for the observation of molecular dynamics and weakly adsorbed, diffusing molecules. HS-AFM has provided intuitive views and directly visualized phenomena that were previously described indirectly, answering questions that were challenging to address using other characterization methods.

Keywords: AFM; HS-AFM; macromolecular crystal; S-layer; 2D crystal; protein crystal



Citation: Rotondi, S.M.C.; Ailuno, G.; Mattioli, S.L.; Pesce, A.; Cavalleri, O.; Canepa, P. Morphological Investigation of Protein Crystals by Atomic Force Microscopy. *Crystals* **2023**, *13*, 1149. <https://doi.org/10.3390/cryst13071149>

Academic Editors: Qun Liu, Dianfan Li, Youzhong Guo, Albert Guskov and Michael C. Wiener

Received: 4 July 2023

Revised: 21 July 2023

Accepted: 22 July 2023

Published: 24 July 2023



Copyright: © 2023 by the authors. Licensee MDPI, Basel, Switzerland. This article is an open access article distributed under the terms and conditions of the Creative Commons Attribution (CC BY) license (<https://creativecommons.org/licenses/by/4.0/>).

1. Introduction on Atomic Force Microscope

Introduced in 1986 by Binning et al. [1], the atomic force microscope (AFM) is a powerful tool for obtaining images of intricate surfaces and specimens that is able to provide high-resolution morphological details of biological/soft samples at the nanoscale [2–11]. It can be used to investigate sample morphology from the molecular level up to more than 100 μm [12,13], providing precise visual details over a size range beyond that of most other common techniques. Its lateral resolution is in the order of nanometers, with a height resolution in the range of hundreds of pm [14–16].

AFM can examine samples of different stiffness, regardless of their electrical conductivity, in different environments, from liquid to ultra-high vacuum. This wide range of operating conditions offers the possibility of measuring an equally wide range of samples such as cells [17–19], bacteria [20–23], extracellular vesicles [24,25], self-assembled molecular films [26–38], Langmuir–Blodgett films [39–42], supported lipid bilayers (SLB) [43–49], polymers [50–53], oxides [54–57], 2D materials [58–62], and other various materials [63–78].

Due to these characteristics, AFM is also well-suited to the study of biomaterials and hydrated biological specimens, as scanning can be carried out in a fluid environment, and specimens require no freezing, fixing, or staining and suffer no dehydration [18,79–81].

The AFM imaging capability is certainly useful, but its overall value is primarily related to the low perturbative nature of the probe/sample interaction, providing a unique insight into the heterogeneous nature of soft samples [82]. With the aim of minimizing tip/sample interaction forces during scans and thoroughly analyzing multiple surface properties, such as elasticity, viscosity, and adhesion, various working modes have been introduced [83]. These modes range from static methods (contact and noncontact modes) [84,85] to resonance methods such as tapping [86], multifrequency [87,88], ringing [89], and contact resonance [90,91]. After the first studies focused on AFM as an imaging technique, a study from Radmacher et al. [92] introduced the force volume (FV) mode, which allowed for the contextual acquisition of morphological and mechanical properties of the analyzed surface. Following the FV, other ramping acquisition modes were introduced, such as Pulse-Force, HarmoniX, PeakForce Quantitative Nanomechanical Mapping (PF-QNM) [82,93,94], and Quantitative Imaging (QITM) [95,96]. It is worth noting that, in many cases, the proper analytical model is needed to obtain information on sample properties such as adhesion and Young's modulus [82].

Despite being acknowledged as a valuable tool in biological sciences, AFM's low imaging speed made it impossible to observe molecular dynamics and weakly adsorbed, diffusing molecules. Several groups attempted to improve AFM imaging speed [97–101], until Ando's group accomplished the first subsecond high-speed-AFM (HS-AFM) imaging on biological samples [102]. Technical developments such as improved feedback and force control have allowed weak interactions between biological macromolecules to be studied without significant perturbation. The effectiveness of HS-AFM has been proved through imaging studies of the dynamic behavior of various proteins [103,104], demonstrating that HS-AFM can offer intuitive views by directly visualizing phenomena that were previously described indirectly, and answering questions that were previously difficult to address using other methods.

In this work, we will review the advantages of using AFM on macromolecular crystal structures and show how the evolution of the technique has allowed the assessment of subtle features of these systems. In particular, the introduction of HS-AFM has overcome previous limitations, enabling the observation of dynamic processes in real space and real time. This review can be of great interest to specialists in the field and even more to those beginning to conduct research in the field of macromolecular crystal investigations.

2. Protein Crystal: From Molecule Distribution to Surface Morphology with AFM

A key process in the crystal growth of both inorganic and macromolecular crystals like proteins, nucleic acids, and virus crystals is the formation and growth of step edges [14]. It is indeed in the investigation of step-edge growth that a real-space imaging method like AFM can provide the most useful information.

The two primary mechanisms that govern the formation of step edges are growth via screw dislocation and growth via the spontaneous emergence of two-dimensional nuclei on active surfaces. A third mechanism known as normal growth does not result in layer addition. Instead, it relies on intense random nucleation on active crystals that possess an unusually low surface free energy. While this mechanism is infrequent, it has been observed in several macromolecular crystals [14].

In addition to the previous mechanisms, a fourth mechanism, not observed in conventional crystal growth, comes into play for macromolecular crystals due to the distinctive properties of concentrated macromolecular solutions [105]. AFM studies focusing on protein crystal growth dating back to the 1990s [2,3,105–115] revealed the presence of multilayer stacks of monomolecular protein layers. These stacks can form hillocks, with shapes that usually reflect the overall morphology of the crystal. The local supersaturation of the molecular solution in the droplet stimulates the crystal epitaxial growth, resulting in the formation of multilayer stacks [116–118]. Each layer provides step edges, allowing for tangential growth and development of new terraces [105]. Moreover, contaminants in the

growth solution (foreign microcrystals, dust, and other contaminating macromolecules) can be incorporated, causing dislocations and morphological defects [110].

An interesting example of the use of AFM for the analysis of macromolecular crystal growth was reported by McPherson et al. [119]. Figure 1A shows the morphology of a typical dislocation of a lysozyme crystal grown with the supersaturation technique and acquired in AFM contact mode. As reported by the authors, the dislocation was the starting point that triggered the step-bunching process. Another application of the AFM on a lysozyme crystal was performed by Mollica et al. [120]. Differently from previous works that investigated the (110) face of lysozyme crystals [3,112,121], the novelty of Mollica et al. was the study of the (101) face. The investigation, performed by tapping mode AFM, revealed an anisotropic growth with a two-dimensional nucleation, as suggested by the terrace morphology visible in Figure 1B.

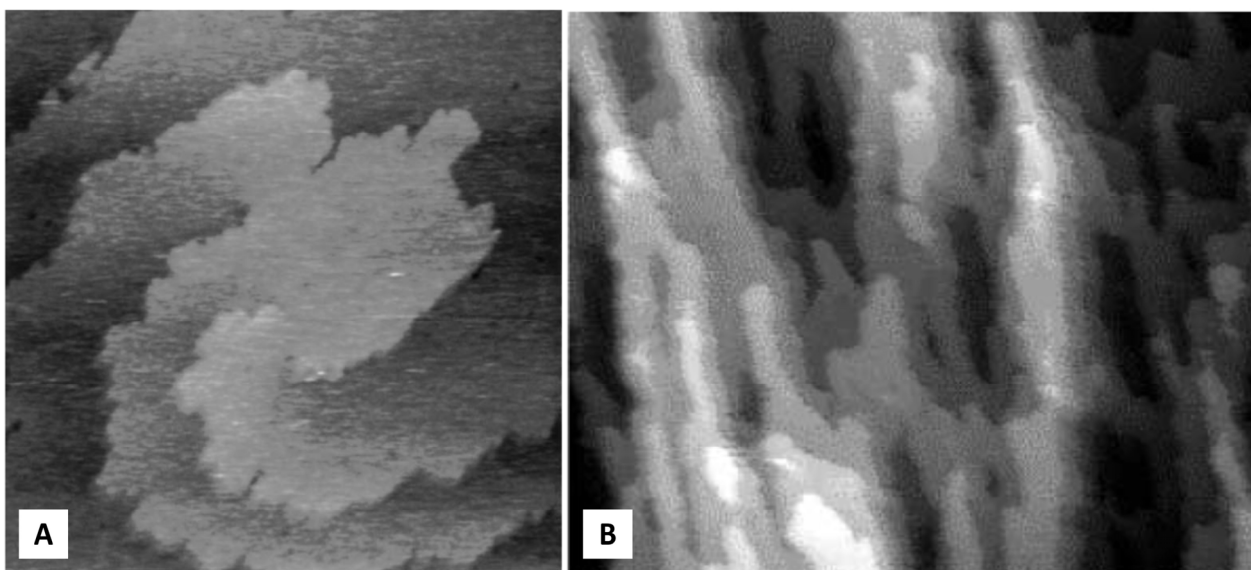


Figure 1. (A) A representative AFM contact-mode image of a complex dislocation structure on the lysozyme crystal surface. Image size is $2.5 \mu\text{m} \times 2.5 \mu\text{m}$. Reprinted with permission from Ref. [119], 1999, *Journal of Crystal Growth*. (B) A representative AFM tapping mode in situ image of a lysozyme (101) crystal face showing the growth islands elongated in the (010) direction. Image size is $2.5 \mu\text{m} \times 2.5 \mu\text{m}$. Reprinted with permission from Ref. [120], 2001, *Eur Biophys J*.

Leveraging the AFM capability to measure the z profile of samples, the authors reported a step height histogram which showed a bimodal distribution, with the Gaussian fit indicating step height values of approximately 3.1 nm and 6.7 nm. These values correspond well to the step heights expected for monomolecular and bimolecular steps in the (101) crystal face (3.4 nm and 6.8 nm, respectively) calculated from the parameters of the tetragonal unit cell of lysozyme crystals. The step height distribution suggests that, unlike the (110) face, the terraces of the (101) face are mostly due to single-molecule steps, as was previously observed through electron microscopy [122] and AFM [119].

The resolution of an AFM image can be pushed further to reach molecular resolution over a crystal face. The work by Mollica et al. [120] demonstrated molecular resolution on the (111) face of a ferritin crystal (Figure 2A). The $450 \text{ nm} \times 400 \text{ nm}$ image allows for the observation of the surface structure at the molecular level, revealing fine details of the terraces. Consistent with the (111) face of a face-centered cubic (fcc) crystal, a hexagonal molecular packing is observed. To determine the lattice symmetry and spacing, the authors performed a two-dimensional Fourier transform analysis on image portions corresponding to single terraces. The value obtained for the lattice constant (13.1 nm) was in good agreement with the 13.0 nm lattice constant calculated from X-ray diffraction experiments.

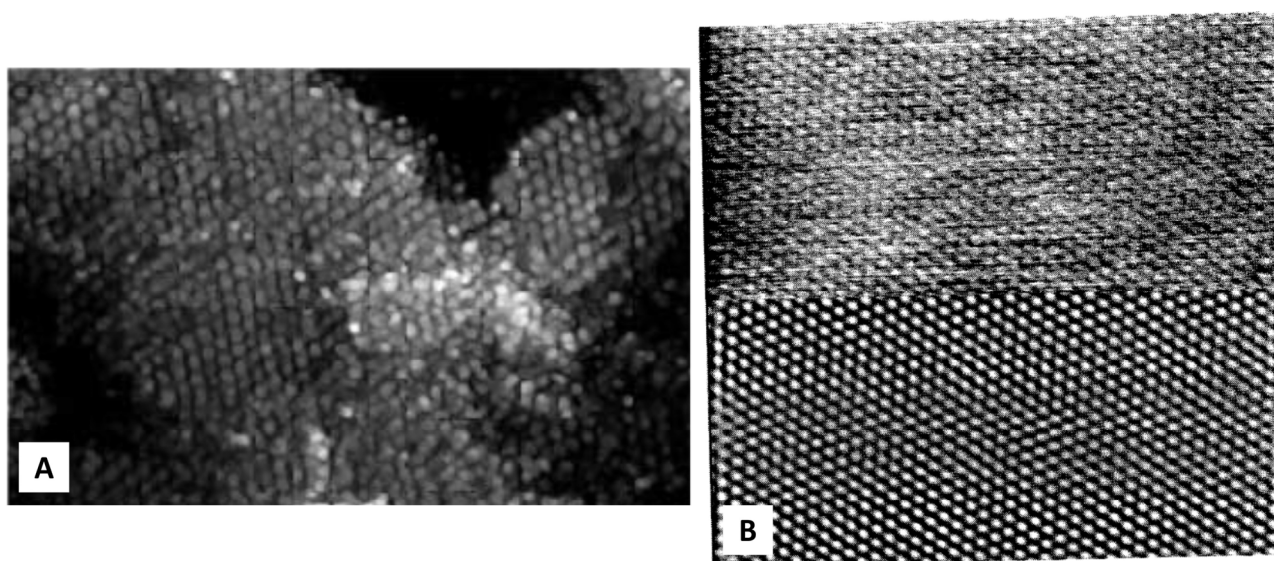


Figure 2. (A) A representative molecular-resolution tapping-mode AFM image of a ferritin crystal (111) face with visible monomolecular islands. Image size is $400\text{ nm} \times 400\text{ nm}$. Reprinted with permission from Ref. [120], 2001, *Eur Biophys J*. (B) A representative contact-mode AFM image of the STMV cubic crystal (111) plane, with its Fourier-filtered image in the lower part. Image size is $1\text{ }\mu\text{m} \times 1\text{ }\mu\text{m}$. Reprinted with permission from Ref. [119], 1999, *Journal of Crystal Growth*.

The importance of AFM in achieving molecular-level details of protein crystals was underlined also by the study by Malkin et al. [106] investigating the satellite tobacco mosaic virus (STMV). Earlier studies on STMV analyzed the aggregation pathway leading to the formation of 3D critical nuclei using quasi-elastic light scattering (QELS) [123] and investigated crystallization kinetics using Michelson interferometry [124]. The authors focused their attention on the growth mechanisms and molecular-scale processes involved in the development of the (111) face of cubic STMV crystals. Figure 2B shows a $1\text{ }\mu\text{m} \times 1\text{ }\mu\text{m}$ AFM image of the (111) plane of a cubic STMV crystal, revealing the individual virus monomers with a center-to-center distance of 18 nm. The lower part of the image has been Fourier-filtered for clarity. Although the structure of the orthorhombic form of STMV had been determined [125], the packing and position of the virus particles in the unit cell were unknown for the cubic crystal form, which was determined to have space group P23 and unit cell parameters of $a = b = c = 25.7\text{ nm}$ through X-ray diffraction experiments [126]. The hexagonal array and intermolecular spacing revealed by the AFM images of the (111) plane indicate that molecules are packed into an fcc lattice, which was impossible to determine from the X-ray data due to the lack of fourfold symmetry in the STMV molecule itself.

The potential of AFM as a tool for surface molecular structure analysis has been illustrated in more recent works by Guo et al. [127]. After successful acquisition of the surface lattice structures of L-valine, D-valine, and D-alanine crystals [128], the authors employed AFM to capture, for the first time, images of the surface-ordered lattices of single crystals of DL-valine and L-alanine [127].

The molecular-resolution images are in excellent agreement with the simulated models, showing the exceptional capability of AFM in investigating the surface molecular structures of amino acid crystals.

The AFM image acquired of the DL-valine crystal (Figure 3A) displays a valine molecule as a single protrusion. Despite attempts to obtain more detailed information from a higher-resolution AFM image (Figure 3B), submolecular resolution could not be achieved, and an accurate description of the submolecular structure of a valine molecule remains challenging. The AFM image of an L-alanine crystal (Figure 3C) reveals easily distinguishable parallel molecular rows of different levels of brightness, forming a periodic structure composed of four molecular chains per unit cell (outlined by a white box in

the figure). The inset of the image presents the Fourier transform pattern of the data. To enhance the periodic features, the original image was Fourier-filtered, resulting in the processed image shown in Figure 3D, which retains only the spectral peaks in the Fourier transform.

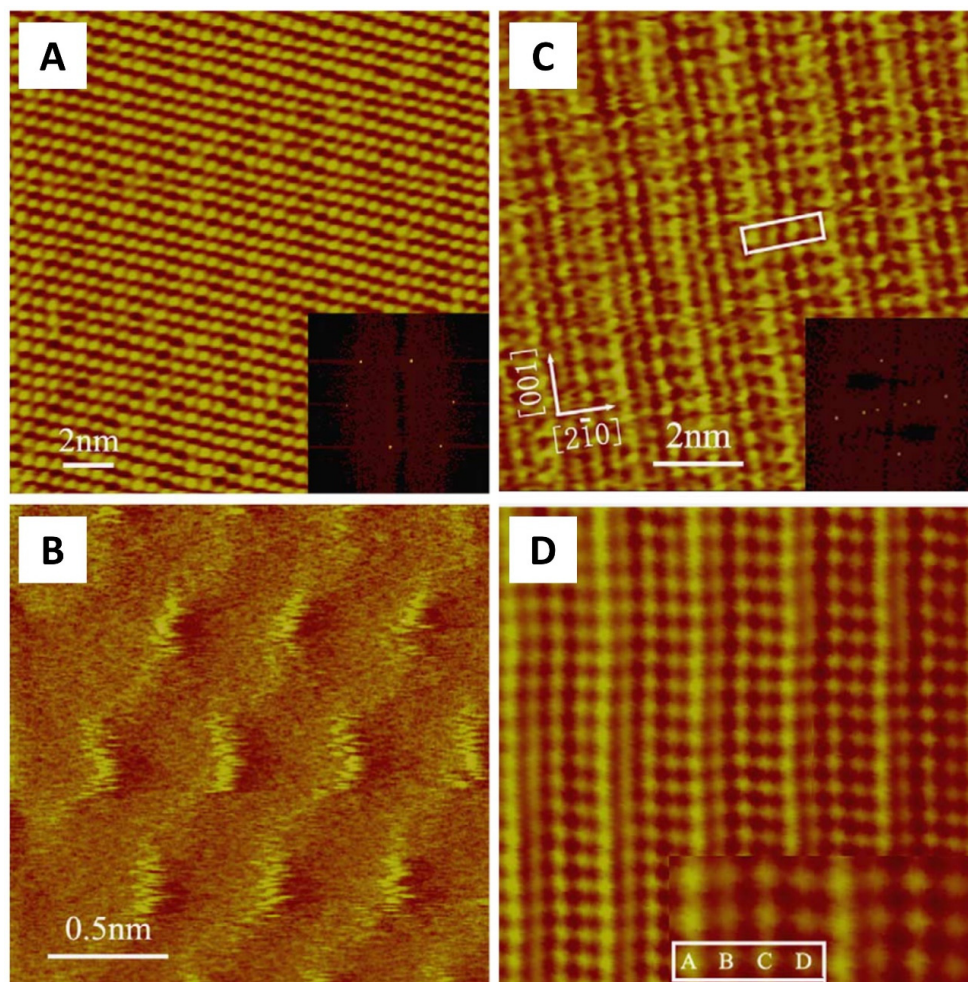


Figure 3. (A) AFM image of DL-valine crystal (001) face in a $18 \text{ nm} \times 18 \text{ nm}$ scan size (fast Fourier transform in the inset). (B) AFM image of (001) face of DL-valine crystal with a higher resolution, scanning area of $2 \text{ nm} \times 2 \text{ nm}$. (C) AFM image of (120) face of L-alanine crystal with a unit cell formed from four molecules contained in the white rectangular frame (fast Fourier transform in the inset). Scanning area of $11 \text{ nm} \times 11 \text{ nm}$. (D) The Fourier-filtered image after rotation and cropping from the original image (A). The inset reports an enlargement with the four molecules of a unit cell indicated by A, B, C and D in the white square. Reprinted with permission from Ref. [127], 2004, *Surface Science*.

The study from Guo et al. showed that AFM is a powerful tool for measuring the surface structure of single crystals.

3. S-Layers

The capability of AFM to produce molecularly resolved images of protein assemblies, previously discussed in the case of 3D protein crystals, can be advantageously exploited to investigate also 2D supramolecular ordered architectures.

The first molecular level AFM studies were reported by Ohnishi et al. in 1992 [129] and Furuno et al. in 1998 [130]. The protein quaternary structure was successfully resolved by Ohnishi et al. in 1993 [131].

A remarkable example of 2D protein architectures are the so-called S-layers, which are two-dimensional arrays of proteinaceous subunits that form surface layers [132]. The S-layers, firstly described as “macromolecular monolayers” by Houwink and Le Poole in [133], have now been identified in hundreds of different species of bacterial and archaeal species [134–141]. S-layers can have different functions, such as protection, adhesion, and cell shape determination. S-layer proteins are excellent model systems for exploring the synthesis, secretion, and assembly of extracellular proteins, and are one of the most abundant biopolymers on Earth [142]. These protein layers consist of a single molecular species that can assemble on the cell surface into closed regular arrays in a low free-energy arrangement.

S-layer properties can moreover be changed due to environment chemical modifications, emphasizing the versatility and significance of S-layers as a building block for constructing supramolecular complex structures that involve proteins, lipids, glycans, and nucleic acids [143–147]. Considering their unique structural and physicochemical properties, S-layers have shown great potential in various fields of application including nano(bio)technology, design of vaccines, diagnostics, and drug delivery [148–152].

Various electron microscopy studies on S-layers have been reported in the literature; they require sample preparation such as thin-sectioning, freeze-etching, freeze-drying, and negative staining [135,153–157]. On the other hand, AFM has proved to be a very versatile analytical tool, with the advantage, over other techniques, of allowing for in situ experiments under controlled conditions in the growth environment [158–168].

An example of the high-resolution capability of AFM applied to S-layers can be found in the work by Scheuring et al. [168]. The authors studied the S-layer formed by the PS2 protein, responsible for the S-layer formation of the *Corynebacterium glutamicum* [169–171]. A hydrophobic amino acid stretch of 21 residues is present at the C-terminus of the protein. When the S-layer is proteolyzed, this C-terminus is removed, which results in detachment of the S-layer from the cell. Bacteria that express the truncated PS2 protein cannot assemble the S-layer and release PS2 into the medium, which confirms the role of the C-terminus in S-layer/cell wall attachment [171].

In the reported work [168], both native and trypsin-treated forms were analyzed, revealing differences in their adsorption behavior. AFM acquisitions showed two different surface types, a flower-shaped one (Figure 4A, left part) and a triangular one (Figure 4A, right part), with a thickness of 4.6 nm for the native and 4.1 nm for the proteolyzed sample. Electrostatic balancing was employed to minimize the tip–sample interaction, allowing for high-resolution topography down to 1 nm [172]. The height information from both surfaces (section analysis reported in Figure 4B) spanned the total height of the S-layer, allowing for a first-time reconstruction of a three-dimensional model from AFM topography.

The study showed evidence of the different behavior of the two sides of the native S-layer in terms of hydrophilicity/hydrophobicity. This property generates the tendency to stack into double-layered assemblies that could be dissected using the AFM tip [173–175].

Another highly studied system is the SbpA protein from *Lysinibacillus sphaericus* (CCM2177), whose reassembly in S-layers on mica does not follow the classical pathway of crystal growth. In this case, a kinetic trap may hinder the reassembly into extended matrices [176], and SbpA proteins can self-assemble into a square lattice symmetry by diffusion from solution to the surface [176,177]. Moreover, the SbpA proteins follow a two-stage nucleation process [166,176], and the protein–substrate and protein–protein interactions may play a role in the assembly pathway [178].

The role that the hydrophobicity of the surfaces has on the SbpA adsorption kinetics was investigated by Herrera et al. [162]. Their investigation was intended to fill the gap in knowledge on the recrystallization kinetics of S-proteins on functional thiols. Indeed several studies had already addressed that aspect on solid and soft interfaces [160,166,178,179].

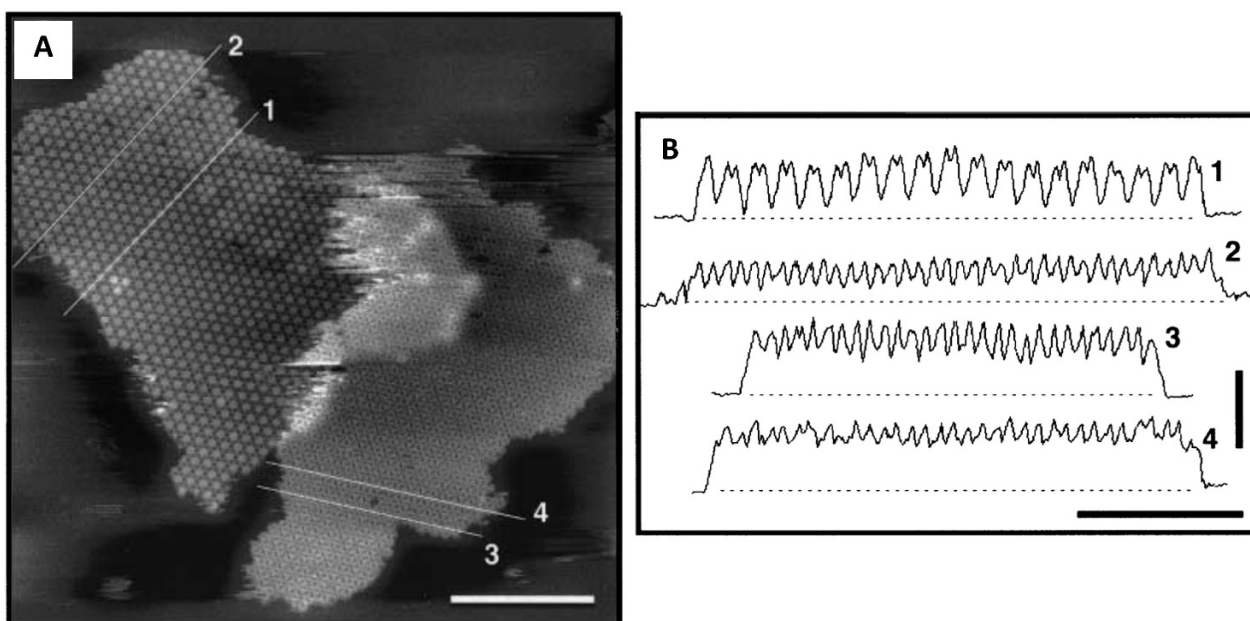


Figure 4. (A) AFM image of two trypsin-treated S-layer patches adsorbed on mica. The left part reports the flower-shaped surface, and the right part, the triangular-shaped one (scale bar 200 nm, z-scale 5 nm). (B) Section analysis corresponding to the numbered lines in (A). In particular: the flower-shaped surface (line 1), the connection arms between the flower-shaped (line 2), the triangular surface (line 3), the backside of the flower-shaped surface in between the triangles (line 4) (scale bar 100 nm, z-scale 5 nm). Reprinted with permission from Ref. [168], 2002 *Molecular Microbiology*.

In their paper [162], the authors investigated how surface modification affects the adsorption rate of S-layer proteins and the formation of protein crystals. They functionalized gold substrates with various alkanethiols with different hydrophobic properties and surface charges, including five types of self-assembled monolayers with methyl, hydroxyl, carboxylic acid, and mannose terminal functional groups.

Protein adsorption rates were faster on uncharged hydrophobic substrates compared to hydrophilic ones. Small S-layer domains were observed on hydrophobic substrates, whereas on OHC₁₁S substrates, the protein adsorbed without forming crystalline layers. When SbpA interacted with a hydrophilic ManC5S surface, partial S-layer recrystallization occurred, but no specific carbohydrate/protein interaction was observed. However, decreasing the pH from 9 to 5 induced different S-layer recrystallization pathways, demonstrating that electrostatic interactions between SbpA and the COOHC₁₁S substrate can tune the adsorption rate. Another interesting result was the dependence of the structure of the protein crystal domains on concentration and surface chemistry. For hydrophobic substrates, concentration helped to enlarge the crystalline domain area, while for COOHC₁₁S substrates, the protein concentration had no influence on the domain size.

Some years later, the same authors [163] explored the role played by protein concentration and observation time on the adsorption of SbpA proteins on hydrophobic SiO₂. AFM measurements were performed using four protein concentrations (from 0.08 μ M to 0.8 μ M) and five different time sequences. The results showed that the rate of adsorption, the nucleation points, and the crystal growth were influenced by the protein–surface interactions, with protein concentration being a crucial factor. Therefore, any alteration in experimental conditions would impact the protein–substrate interactions, highlighting their significance in the formation of crystal layers. The observation time influenced the formation of 2D crystals, with nucleation points and protein domain size increasing with time. The lowest concentration did not form a confluent protein layer, while the highest concentration completely covered the substrate surface. A sum-up of the results is presented in Figure 5.

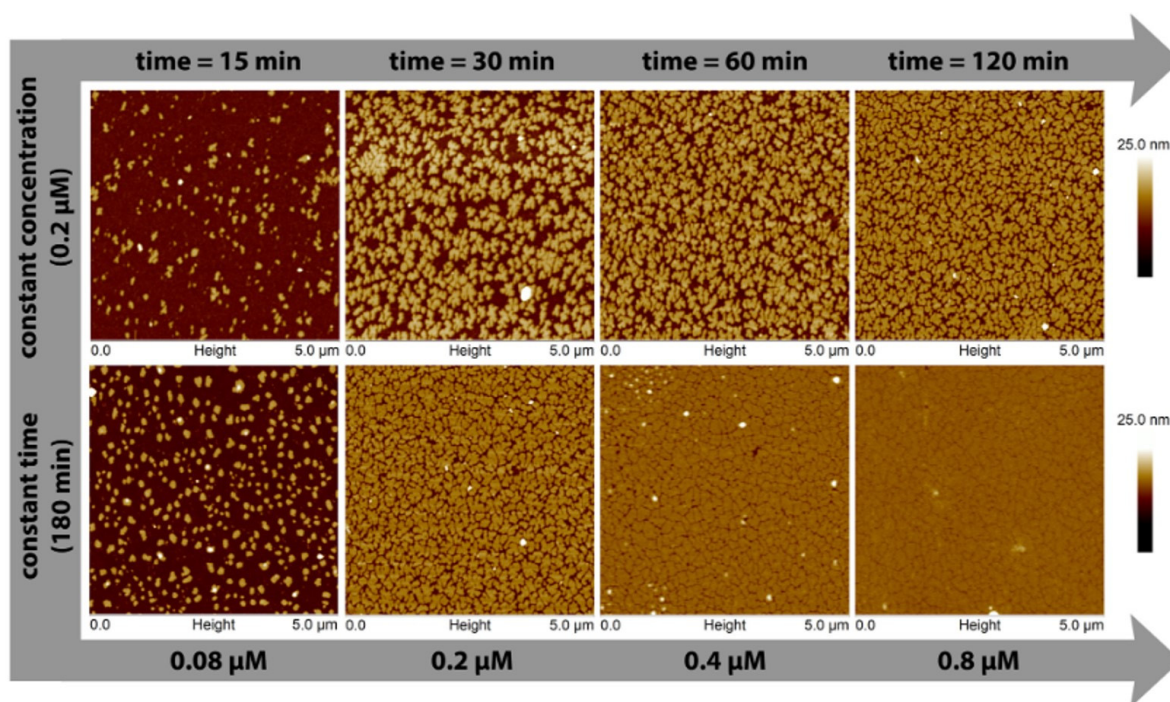


Figure 5. In situ AFM images showing (upper row) the SbpA layer time evolution with a starting protein concentration of $0.2 \mu\text{M}$, and (bottom row) the influence of the initial protein concentration after 180 min. Reprinted with permission from Ref. [163], 2018, *Microsc ResTech*.

The AFM phase images confirmed that a more compact protein layer was achieved at higher concentrations, as the gaps between the growing crystalline domains were reduced. The results also showed that the best resolution in AFM imaging is obtained at higher protein concentrations (harder surfaces), confirming previous observations that sample softness affects AFM resolution [180]. The authors reported that the main limitation to the experimental procedure was the rapid adsorption kinetics of the SbpA protein on these surfaces. The AFM imaging started after the hydrophobic surface had already been exposed to the protein solution for about 15 min, which was enough time for the smallest crystalline domains to form. While the initial adsorption and recrystallization steps were not directly visualized by AFM, previous QCM-D results indicated that the process is primarily governed by protein–substrate interactions, followed by subsequent protein self-assembly.

The AFM capability of surface analysis at the molecular scale and at timescales typical for protein crystallization was exploited also by Vekilov et al. [164]. The aim of their experiments was to gain insight into the nucleation pathways by imaging clusters for the crystallization of a model protein system. In situ AFM was performed in supersaturated solutions to monitor the growth of clusters on the bottom of the AFM cell. The authors focused on apoferritin, a protein consisting of 24 subunits arranged in pairs along the 12 walls of a quasi-rhombo-dodecahedron [181–183]. Apoferritin crystals have a face-centered cubic lattice exposing (111) planes with a hexagonal molecular packing [184,185].

The authors observed the adsorption of a disordered monomolecular protein layer covering the entire glass surface. Throughout the experiment, no partial or full second layer of adsorbed molecules was observed, and there were no changes in the molecular arrangements. Therefore, it was concluded that the apoferritin molecules were rigidly attached to the glass substrate, allowing for the imaging of individual molecules and determination of their size, which was found to be approximately 13 nm, as observed in crystals [185].

The images in Figure 6A–D show typical clusters adsorbed on the protein monolayer covering the AFM cell bottom. The two considered clusters contain four and nine molecules,

respectively. According to nucleation theories, the smaller cluster is expected to disappear quickly, while the larger one should be closer to a labile equilibrium with the solution [186]. However, Figure 6A–D show that the smaller cluster gains and loses two molecules, ultimately retaining four molecules after about 20 min of observation. Conversely, the larger cluster dissolves progressively over the same period. This apparent contradiction is explained by the fact that nucleation theories describe the evolution of large populations of clusters, and the fate of individual clusters is determined by a random sequence of events. The authors suggested that their findings may have implications for understanding and predicting the behavior of ensembles of small aggregates driven by surface energy, with implication in nanotechnologies [187].

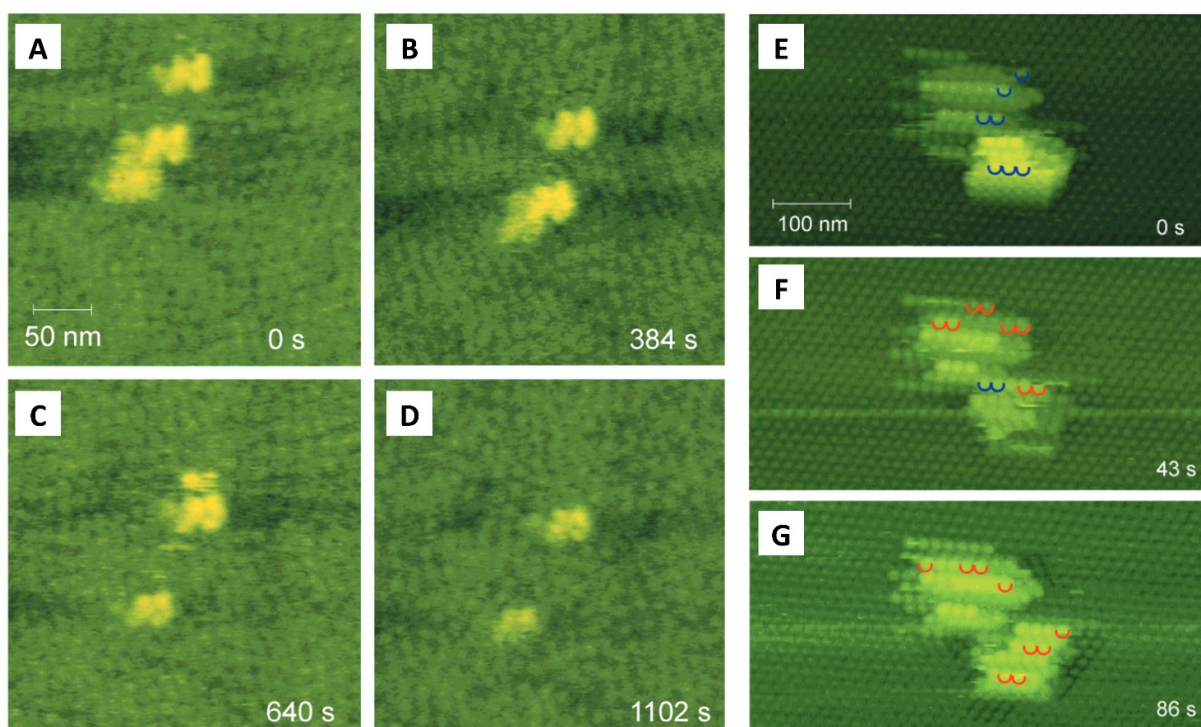


Figure 6. (A–D) AFM images showing the evolution of two adsorbed protein clusters on the substrate. (E–G) AFM images showing the dynamics of protein exchange between a typical protein cluster and the solution (the molecules that are missing from or appear in the cluster with respect to the next frame are highlighted, respectively, in blue and in red). Reprinted with permission from Ref. [164], 2001, *J. Am. Chem. Soc.*

Another example of molecule exchange dynamics between clusters and solution is presented in Figure 6D–F. In this case, the lower level in the images represents the surface of a large apoferritin crystal, with an on-top cluster of apoferritin with the same molecular arrangement of the underlying crystal [188,189]. The molecules in the cluster are organized in rods of four to eight molecules, with the center-to-center distance between adjacent molecules in a rod equal to that along the close-packed (110) direction in the crystal lattice. The three subsequent images acquired on the cluster (Figure 6D–F) show that molecules attach and detach from the cluster with comparable frequencies. From the low net exchange rate between the cluster and the solution, the authors inferred that the size of the considered cluster was slightly above the critical size for the saturation condition.

4. Real-Time Visualization of Biomolecular Dynamic: High-Speed AFM

Although AFM has been widely recognized as a powerful tool in the biological sciences, its limited imaging speed (tens of seconds to minutes to complete one image) has hindered its widespread use compared to other popular techniques like optical micro-

scopies. In many cases, understanding the assembly process and the molecular dynamics at their very initial step is crucial for understanding the biological processes that occur within living cells, such as molecular interactions and conformational changes. To overcome the above-mentioned slow imaging speed limits, several research groups have worked to increase the imaging speed of AFM [97–102,190], and high-speed atomic force microscopy (HS-AFM) was developed. The use of tapping mode [191] to reduce lateral forces during scans, miniaturized cantilevers, high-frequency feedback systems, and newly developed amplitude detectors [192,193] allow the current HS-AFM to capture images at a speed in the range of 30–60 ms per frame with a scan size of about 250 nm and 100 scan lines under typical conditions for biomolecular investigations [104,194].

Based on these characteristics, HS-AFM was employed, e.g., to observe the conformational changes of proteins [15,195–208], to monitor enzyme reactions [209–213], to study the growth of amyloid-like fibrils [214–216], to investigate the DNA conformational changes [217–219], and to follow protein dynamics while interacting with other proteins [220–224] or with membranes [225–233]. In addition to imaging applications, HS-AFM has been shown to be valuable for high-speed force spectroscopy (HS-FS) and active high-frequency microrheology (HF-MR) [234–238]. These advancements have enabled the exploration of previously unattainable dynamic ranges, enabling experimental protein unfolding studies that can be directly compared to molecular dynamics simulations [234,235].

Furthermore, recent advancements in HS-AFM have provided valuable insights into the molecular mechanisms of cyclic nucleotide-gated (CNG) channels, as investigated in the work from Marchesi et al. [239]. In their work, the authors studied the bacterial SthK CNG, chosen as a model CNG channel that is important for linking intracellular cyclic nucleotide signaling with electrical signaling at the cell membrane [240–243]. These channels are regulated by the binding of cyclic nucleotides (cAMP or cGMP) to a specific intracellular domain called the cyclic nucleotide-binding domain (CNBD) [244,245]. This binding induces conformational changes that open or close the channel pore, controlling the flow of ions across the membrane. These channels, which are crucial for neuronal excitability and sensory pathways [246,247], consist of tetrameric subunit arrangements surrounding a central pore [248]. HS-AFM has enhanced our understanding of the dynamic behavior and functional properties of CNG channels, revealing their physiological roles and molecular mechanisms. In particular, studies demonstrated that cGMP does not activate SthK channels but instead inhibits the cAMP-induced activity, leading to channel closure [249,250]. In the work of Ruan et al. [197], the authors utilized HS-AFM to observe the transition of SthK channels from an activated/open state to a resting/closed state by adding an excess amount of cGMP. Starting with an initial concentration of 0.1 mM cAMP, increasing concentrations of cGMP were added until reaching a final concentration of 7 mM. The imaging revealed a noticeable change in the surface topography and in the two-dimensional crystal packing. This change originated from the molecules located at the border of the crystal patch and gradually propagated towards the center with slow kinetics, as can be clearly observed in Figure 7A from left (0.1 mM cAMP) to right (7 mM cGMP).

Analyzing the morphological changes of the SthK, the authors concluded that upon the transition from a closed to an open state, the four CNBDs that form the channel undergo distinct structural changes. These CNBDs move vertically towards the membrane by approximately 0.6 nm and spread out by approximately 0.4 nm. Additionally, they rotate relative to the pore domain. Structural analysis suggested that this rotation of the CNBDs, triggered by cAMP activation, results in a displacement of approximately 1.3 nm on the periphery of the C-linker. This movement is transmitted through the C-linker to the pore domain, leading to the opening of the channel pore.

These observations suggested that the long-range interactions between adjacent and distant protein domains are responsible for structural transitions not only of cyclic nucleotide-modulated channels but also of other channels controlled by the binding of small intracellular ligands to carboxyl terminal regulatory domains. This indicates a shared mechanism for conformational changes and functional regulation among these channels.

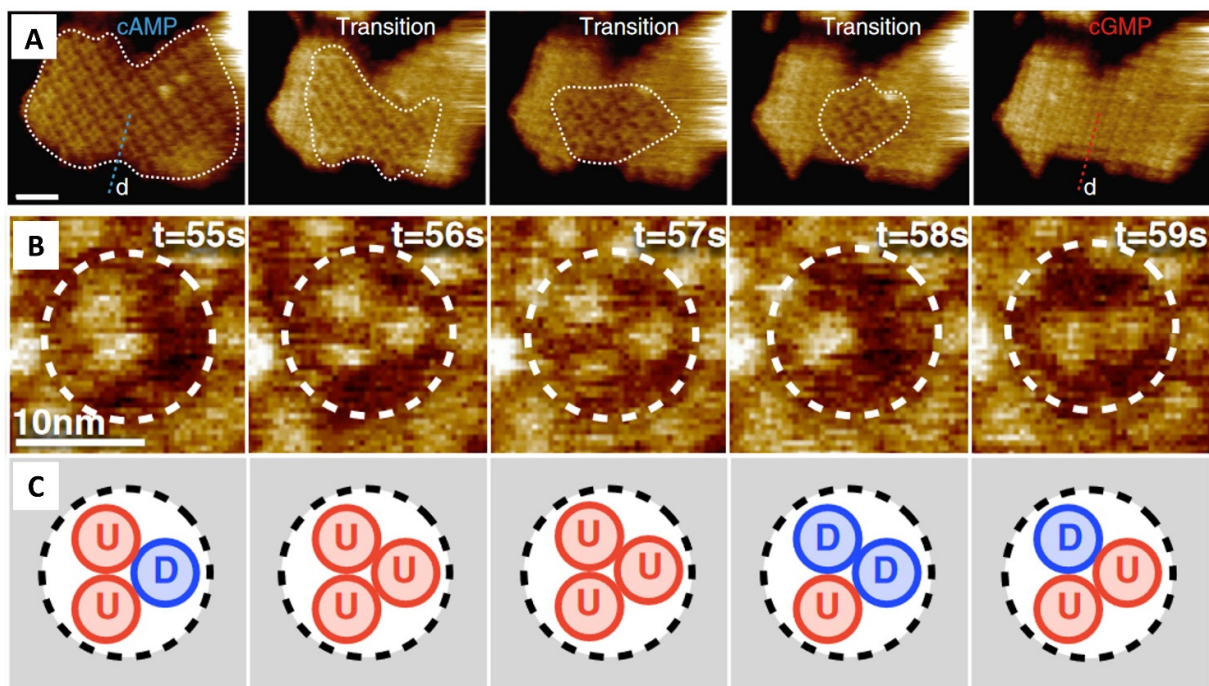


Figure 7. (A) Real-time HS-AFM imaging showing the dynamics of ligand-induced conformational changes in SthK, with an initial 0.1 mM cAMP to a final 7 mM cGMP. The SthK channels' conformational changes are outlined with a dotted line. Scale bar 30 nm. Reprinted with permission from Ref. [239], 2018, *Nature Communications*. (B) HS-AFM imaging sequential frames showing conformational changes of GltPh trimers. (C) A schematic representation of the up (U) or down (D) state of each protomer of the AFM images presented in (B). Reprinted with permission from Ref. [197], 2017, *PNAS*.

Alongside membrane channels, which passively allow or block the transport of solutes through membranes, a different assisted mechanism of intra/extramembrane communication is represented by the membrane transporters [251].

Between them, extensive research has been performed on glutamate, a membrane transporter that plays a crucial role in maintaining appropriate glutamate levels in the synaptic cleft to prevent excitotoxicity [252]. Dysfunctions in these transporters are linked to various neurological disorders including epilepsy, Alzheimer's disease, and amyotrophic lateral sclerosis [253]. The elucidation of the crystal structures of the glutamate transporter homolog from the archaeobacterium *Pyrococcus horikoshii* (GltPh) has been a significant milestone in understanding the mechanism of ion-coupled transport. Previous studies on glutamate transporters have provided valuable insights into their localization, function, and structure [254–256]. However, dynamic studies of the transport mechanism have been limited, making HS-AFM observations a valuable contribution to understanding the functioning of glutamate transporters. In this direction, a recent study from Ruan et al. [197] exploited HS-AFM to obtain direct insights into the dynamic behavior of glutamate transporters.

The authors observed a membrane-reconstituted GltPh, whose trimers in the membrane were visualized as formed by three protomers arranged in a triangular pattern with a central cavity. Each protomer was imaged as a ~2 nm diameter and 2 nm height protrusion. These observations suggested that GltPh was exposing the transport domains towards the extracellular side facing the HS-AFM tip. The transport domains exhibited reversible conformational changes between an outward-facing (up) and an inward-facing (down) distinct state. The trimeric structure of the transporter was visible when all the three subunits were in the outward-facing state, with the transport domains clearly protruding from the membrane plane (Figure 7B, with $t = 56$ s and $t = 57$ s). The domains demonstrated

vertical motion, moving up and down with an amplitude of approximately a couple of nm. To better identify the up or down state of each protomer in the AFM images of Figure 7B, a correlated up (u) and down (d) scheme is reported in Figure 7C. These observations were consistent with crystal structures, single-molecule Förster resonance energy transfer, and electron paramagnetic resonance studies [257–263].

To investigate the relationship between molecular motion and function, the GltPh domain movements between the “up” and “down” states were studied under various environmental conditions, including the absence of substrate, different concentrations of Na⁺/Asp, and the presence of an inhibitor (DL-TBOA) [264]. As expected for a Na⁺/Asp symporter, the HS-AFM revealed that GltPh exhibits greater dynamics in the absence and presence of Na⁺ and Asp compared to when only Na⁺ is present. Contextually, when Asp was replaced with the competitive inhibitor, GltPh remained trapped in the outward-facing state with minimal observed movements. Furthermore, analyzing the correlations between the conformations of the protomers within the trimer revealed that each protomer acted independently and without a specific order in terms of their location within the trimeric structure.

The HS-AFM imaging capability has been used also to investigate the structural dynamics of bacteriorhodopsin (bR), a light-driven proton pump [265–268]. Imaging on a slow photocycle bR mutant (D96N), conformational changes in the cytoplasmic domains were observed [201]. Upon light illumination, HS-AFM allowed the observation of approximately 0.8 nm lateral outward displacement of the E–F loops in each bR. This information was correlated with high-resolution electron microscopy and X-ray crystallography data, demonstrating the powerful combination of these techniques in assigning structural dynamics.

The capability of HS-AFM to catch protein dynamics at the single-molecule level has been recently demonstrated by a study on the interaction between spike variants and ACE2 receptors [269]. Hinterdorfer and coworkers [269] could follow the spike trimer dynamics in the presence of ACE2, showing that Delta and Omicron variants enhance viral attachment to the host-cell receptor compared to the early Wuhan-1 isolate. This finding would explain not only the increased rate of viral uptake but also the increased resistance of the variants against host–cell detachment by shear forces.

The above studies highlight the exceptional ability of HS-AFM to investigate dynamic processes involving individual unlabeled proteins. Traditional techniques often struggle to capture conformational changes with high precision due to low signal-to-noise ratios. In contrast, HS-AFM provides a powerful tool to directly observe and characterize these conformational changes, enabling a more detailed understanding of protein dynamic behavior at the single-molecule level.

To underline the importance of the HS-AFM introduction, Table 1 reports some relevant works performed with HS-AFM.

Table 1. Summary of relevant works performed with HS-AFM.

Authors	Studied System
Kodera et al. (2010) [15]	Direct visualization of myosin V molecules walking along actin tracks.
Shibata et al. (2010) [201]	Visualization of the dynamic changes of the light-driven proton pump bacteriorhodopsin upon illumination.
Takahashi et al. (2016) [233]	Observation in real time of lipid bilayers dynamics phase transition from ripple phase to fluid phase reversibly using a newly developed and integrated temperature-control device.
Ruan et al. (2017) [197]	Observations of the transport dynamics of the glutamate transporter homolog in a membrane-reconstituted GltPh.
Heath et al. (2018) [238]	The introduction of HS-AFM height spectroscopy and its application to measure surface concentrations, diffusion rates, and oligomer sizes of annexin-V molecules during membrane binding and self-assembly.
Marchesi et al. (2018) [239]	Observation of the conformational reversible dynamics of a prokaryotic homolog of CNG channels, SthK, upon activation in response to cAMP-binding.
Ruan et al. (2018) [224]	The effect of buffer exchange on structural titration experiments to visualize GLIC gating at the single-molecule level under native conditions.
Zhu et al. (2022) [269]	Visualization of conformational dynamics of isolated spike trimers complexed with their essential entry receptor ACE2.

5. Conclusions

Since its introduction in 1986, AFM has been employed in studying biological samples due to its high-resolution imaging capability and broad scan range. These features, together with the possibility to image samples in liquid, have made AFM a powerful tool for investigating protein crystals directly in their original growth environment. As reported in the present paper, AFM investigations of protein crystals have contributed to elucidating the molecular mechanisms involved in the growth of protein crystals, from the nanoscale level up to hundreds of micrometers.

Moreover, AFM has shown great potential in investigating S-layers at the molecular level, expanding our understanding of their specific biological functions and paving the way to their exploitation as a promising system for various applicative fields including diagnostics, drug delivery, and design of vaccines. Using AFM, the effect on the structure of S-layers induced by the chemical modifications has been investigated live.

The introduction of high-speed AFM has enabled observations of dynamic processes that were previously difficult to investigate. This development has enabled the observation of diffusing molecules and molecular dynamics, providing direct views of phenomena that were previously described indirectly.

HS-AFM, with its unique ability to provide real-space and real-time observations, has been instrumental in tackling challenging areas, such as the measurement of proteins in action, and has therefore proved to be a valuable tool in advancing our understanding of dynamic biological processes.

Given its capability to provide insights into assembly, stability, and interactions of macromolecules on surfaces, the application of HS-AFM to macromolecular crystals could pave the way to the direct observation of crystal growth, enabling the dynamic analysis of surface morphological changes up to the assessment of the dynamic behavior of individual molecules within the crystal lattice. Combining HS-AFM with other techniques, such as X-ray crystallography, will allow us to obtain a more comprehensive understanding of macromolecular crystal structures and their functional properties.

Funding: The authors acknowledge the financial support from Università degli Studi di Genova. This work was performed under the project “Dipartimenti di Eccellenza 2018–2022” of the Italian Ministry of University and Research.

Data Availability Statement: Not applicable.

Conflicts of Interest: The authors declare no conflict of interest.

References

1. Binnig, G.; Quate, C.F.; Gerber, C. Atomic Force Microscope. *Phys. Rev. Lett.* **1986**, *56*, 930–933. [[CrossRef](#)]
2. Durbin, S.D.; Carlson, W.E. Lysozyme Crystal Growth Studied by Atomic Force Microscopy. *J. Cryst. Growth* **1992**, *122*, 71–79. [[CrossRef](#)]
3. Durbin, S.D.; Carlson, W.E.; Saros, M.T. In Situ Studies of Protein Crystal Growth by Atomic Force Microscopy. *J. Phys. D Appl. Phys.* **1993**, *26*, B128. [[CrossRef](#)]
4. Müller, D.J.; Dufrêne, Y.F. Atomic Force Microscopy as a Multifunctional Molecular Toolbox in Nanobiotechnology. *Nat. Nanotechnol.* **2008**, *3*, 261–269. [[CrossRef](#)]
5. Rotondi, S.M.C.; Canepa, P.; Angeli, E.; Canepa, M.; Cavalleri, O. DNA Sensing Platforms: Novel Insights into Molecular Grafting Using Low Perturbative AFM Imaging. *Sensors* **2023**, *23*, 4557. [[CrossRef](#)]
6. Aragno, I.; Odetti, P.; Altamura, F.; Cavalleri, O.; Rolandi, R. Structure of Rat Tail Tendon Collagen Examined by Atomic Force Microscope. *Experientia* **1995**, *51*, 1063–1067. [[CrossRef](#)]
7. Cross, S.E.; Jin, Y.-S.; Rao, J.; Gimzewski, J.K. Nanomechanical Analysis of Cells from Cancer Patients. *Nat. Nanotechnol.* **2007**, *2*, 780–783. [[CrossRef](#)] [[PubMed](#)]
8. Svaldo-Lanero, T.; Krol, S.; Magrassi, R.; Diaspro, A.; Rolandi, R.; Gliozzi, A.; Cavalleri, O. Morphology, Mechanical Properties and Viability of Encapsulated Cells. *Ultramicroscopy* **2007**, *107*, 913–921. [[CrossRef](#)]
9. Dorobantu, L.S.; Gray, M.R. Application of Atomic Force Microscopy in Bacterial Research. *Scanning* **2010**, *32*, 74–96. [[CrossRef](#)]
10. Formosa, C.; Grare, M.; Duval, R.E.; Dague, E. Nanoscale Effects of Antibiotics on *P. Aeruginosa*. *Nanomedicine* **2012**, *8*, 12–16. [[CrossRef](#)]

11. Aguayo, S.; Donos, N.; Spratt, D.; Bozec, L. Single-Bacterium Nanomechanics in Biomedicine: Unravelling the Dynamics of Bacterial Cells. *Nanotechnology* **2015**, *26*, 062001. [[CrossRef](#)] [[PubMed](#)]
12. Willemsen, O.H.; Snel, M.M.E.; Cambi, A.; Greve, J.; De Grooth, B.G.; Figdor, C.G. Biomolecular Interactions Measured by Atomic Force Microscopy. *Biophys. J.* **2000**, *79*, 3267–3281. [[CrossRef](#)] [[PubMed](#)]
13. Canepa, P.; Firpo, G.; Mattera, L.; Canepa, M.; Cavalleri, O. Calcium and Phosphorous Enrichment of Porous Niobium and Titanium Oxides for Biomaterial Applications. *Surf. Coat. Technol.* **2020**, *389*, 125634. [[CrossRef](#)]
14. McPherson, A.; Kuznetsov, Y.G.; Malkin, A.J.; Plomp, M. Macromolecular Crystal Growth Investigations Using Atomic Force Microscopy. *J. Synchrotron Radiat.* **2004**, *11*, 21–23. [[CrossRef](#)] [[PubMed](#)]
15. Kodera, N.; Yamamoto, D.; Ishikawa, R.; Ando, T. Video Imaging of Walking Myosin V by High-Speed Atomic Force Microscopy. *Nature* **2010**, *468*, 72–76. [[CrossRef](#)] [[PubMed](#)]
16. Sokolov, I.Y.; Firtel, M.; Henderson, G.S. In Situ High-resolution Atomic Force Microscope Imaging of Biological Surfaces. *J. Vac. Sci. Technol. A* **1996**, *14*, 674–678. [[CrossRef](#)]
17. Pedraz, P.; Casado, S.; Rodriguez, V.; Giordano, M.C.; de Mongeot, F.B.; Ayuso-Sacido, A.; Gnecco, E. Adhesion Modification of Neural Stem Cells Induced by Nanoscale Ripple Patterns. *Nanotechnology* **2016**, *27*, 125301. [[CrossRef](#)]
18. Peng, Y.; Zhang, J.; Xue, W.; Wu, W.; Wang, Y.; Mei, K.; Chen, Y.; Rao, D.; Yan, T.; Wang, J.; et al. Nanomechanical Vibration Profiling of Oocytes. *Nano Res.* **2023**, *16*, 2672–2681. [[CrossRef](#)]
19. Haase, K.; Pelling, A.E. Investigating Cell Mechanics with Atomic Force Microscopy. *J. R. Soc. Interface* **2015**, *12*, 20140970. [[CrossRef](#)]
20. Liu, S.; Wang, Y. Application of AFM in Microbiology: A Review. *Scanning* **2010**, *32*, 61–73. [[CrossRef](#)]
21. Pelling, A.E.; Sehati, S.; Gralla, E.B.; Valentine, J.S.; Gimzewski, J.K. Local Nanomechanical Motion of the Cell Wall of *Saccharomyces cerevisiae*. *Science* **2004**, *305*, 1147–1150. [[CrossRef](#)] [[PubMed](#)]
22. Huang, Q.; Wu, H.; Cai, P.; Fein, J.B.; Chen, W. Atomic Force Microscopy Measurements of Bacterial Adhesion and Biofilm Formation onto Clay-Sized Particles. *Sci. Rep.* **2015**, *5*, 16857. [[CrossRef](#)] [[PubMed](#)]
23. Doktycz, M.J.; Sullivan, C.J.; Hoyt, P.R.; Pelletier, D.A.; Wu, S.; Allison, D.P. AFM Imaging of Bacteria in Liquid Media Immobilized on Gelatin Coated Mica Surfaces. *Ultramicroscopy* **2003**, *97*, 209–216. [[CrossRef](#)]
24. Parisse, P.; Rago, I.; Ulloa Severino, L.; Perissinotto, F.; Ambrosetti, E.; Paoletti, P.; Ricci, M.; Beltrami, A.P.; Cesselli, D.; Casalis, L. Atomic Force Microscopy Analysis of Extracellular Vesicles. *Eur. Biophys. J.* **2017**, *46*, 813–820. [[CrossRef](#)]
25. Vorselen, D.; Piontek, M.C.; Roos, W.H.; Wuite, G.J.L. Mechanical Characterization of Liposomes and Extracellular Vesicles, a Protocol. *Front. Mol. Biosci.* **2020**, *7*, 139. [[CrossRef](#)] [[PubMed](#)]
26. Pinto, G.; Dante, S.; Rotondi, S.M.C.; Canepa, P.; Cavalleri, O.; Canepa, M. Spectroscopic Ellipsometry Investigation of a Sensing Functional Interface: DNA SAMs Hybridization. *Adv. Mater. Interfaces* **2022**, *9*, 2200364. [[CrossRef](#)]
27. Canepa, P.; Gonella, G.; Pinto, G.; Grachev, V.; Canepa, M.; Cavalleri, O. Anchoring of Aminophosphonates on Titanium Oxide for Biomolecular Coupling. *J. Phys. Chem. C* **2019**, *123*, 16843–16850. [[CrossRef](#)]
28. Liu, J.; Xu, R.; Zhu, Y.; Yang, D.-Q.; Nie, H.-Y.; Lau, W.M. AFM/XPS Analysis of the Growth and Architecture of Oriented Molecular Monolayer by Spin Cast Process and Its Cross-Linking Induced by Hyperthermal Hydrogen. *Appl. Sci.* **2022**, *12*, 6233. [[CrossRef](#)]
29. Pinto, G.; Parisse, P.; Solano, I.; Canepa, P.; Canepa, M.; Casalis, L.; Cavalleri, O. Functionalizing Gold with Single Strand DNA: Novel Insight into Optical Properties via Combined Spectroscopic Ellipsometry and Nanolithography Measurements. *Soft Matter* **2019**, *15*, 2463–2468. [[CrossRef](#)]
30. Canepa, P.; Gregurec, D.; Liessi, N.; Rotondi, S.M.C.; Moya, S.E.; Millo, E.; Canepa, M.; Cavalleri, O. Biofunctionalization of Porous Titanium Oxide through Amino Acid Coupling for Biomaterial Design. *Materials* **2023**, *16*, 784. [[CrossRef](#)]
31. Solano, I.; Parisse, P.; Gramazio, F.; Cavalleri, O.; Bracco, G.; Castronovo, M.; Casalis, L.; Canepa, M. Spectroscopic Ellipsometry Meets AFM Nanolithography: About Hydration of Bio-Inert Oligo(Ethylene Glycol)-Terminated Self Assembled Monolayers on Gold. *Phys. Chem. Chem. Phys.* **2015**, *17*, 28774–28781. [[CrossRef](#)] [[PubMed](#)]
32. Barrena, E.; Ocal, C.; Salmeron, M. Structure and Stability of Tilted-Chain Phases of Alkanethiols on Au(111). *J. Chem. Phys.* **2001**, *114*, 4210–4214. [[CrossRef](#)]
33. Toccafondi, C.; Prato, M.; Maidecchi, G.; Penco, A.; Bisio, F.; Cavalleri, O.; Canepa, M. Optical Properties of Yeast Cytochrome c Monolayer on Gold: An in Situ Spectroscopic Ellipsometry Investigation. *J. Colloid Interface Sci.* **2011**, *364*, 125–132. [[CrossRef](#)] [[PubMed](#)]
34. Fujita, A.; Kobayashi, K.; Yamada, H. Investigation of Local Hydration Structures of Alkanethiol Self-Assembled Monolayers with Different Molecular Structures by FM-AFM. *Langmuir* **2018**, *34*, 15189–15194. [[CrossRef](#)]
35. Pillai, S.; Pai, R.K. Controlled Growth and Formation of SAMs Investigated by Atomic Force Microscopy. *Ultramicroscopy* **2009**, *109*, 161–166. [[CrossRef](#)]
36. Bueno, O.V.M.; Benítez, J.J.; San-Miguel, M.A. Understanding Segregation Processes in SAMs Formed by Mixtures of Hydroxylated and Non-Hydroxylated Fatty Acids. *RSC Adv.* **2019**, *9*, 39252–39263. [[CrossRef](#)] [[PubMed](#)]
37. Canepa, P.; Solano, I.; Uttiya, S.; Gemme, G.; Rolandi, R.; Canepa, M.; Cavalleri, O. Phosphonate Molecular Layers on TiO₂ Surfaces. *MATEC Web Conf.* **2017**, *98*, 03001. [[CrossRef](#)]
38. Buzio, R.; Gerbi, A.; Barra, M.; Chiarella, F.; Gnecco, E.; Cassinese, A. Subnanometer Resolution and Enhanced Friction Contrast at the Surface of Perylene Diimide PDI8-CN2 Thin Films in Ambient Conditions. *Langmuir* **2018**, *34*, 3207–3214. [[CrossRef](#)]

39. Chi, L.F.; Anders, M.; Fuchs, H.; Johnston, R.R.; Ringsdorf, H. Domain Structures in Langmuir-Blodgett Films Investigated by Atomic Force Microscopy. *Science* **1993**, *259*, 213–216. [[CrossRef](#)]
40. Gupta, R.K.; Suresh, K.A. AFM Studies on Langmuir-Blodgett Films of Cholesterol. *Eur. Phys. J. E* **2004**, *14*, 35–42. [[CrossRef](#)]
41. Hagedorn, S.; Drolle, E.; Lorentz, H.; Srinivasan, S.; Leonenko, Z.; Jones, L. Atomic Force Microscopy and Langmuir-Blodgett Monolayer Technique to Assess Contact Lens Deposits and Human Meibum Extracts. *J. Optom.* **2015**, *8*, 187–199. [[CrossRef](#)] [[PubMed](#)]
42. Garcia-Manyes, S.; Domènech, Ò.; Sanz, F.; Montero, M.T.; Hernandez-Borrell, J. Atomic Force Microscopy and Force Spectroscopy Study of Langmuir-Blodgett Films Formed by Heteroacid Phospholipids of Biological Interest. *Biochim. Biophys. Acta (BBA)—Biomembr.* **2007**, *1768*, 1190–1198. [[CrossRef](#)] [[PubMed](#)]
43. Rispoli, P.; Carzino, R.; Svaldo-Lanero, T.; Relini, A.; Cavalleri, O.; Fasano, A.; Liuzzi, G.M.; Carlone, G.; Riccio, P.; Gliozzi, A.; et al. A Thermodynamic and Structural Study of Myelin Basic Protein in Lipid Membrane Models. *Biophys. J.* **2007**, *93*, 1999–2010. [[CrossRef](#)]
44. Lv, Z.; Banerjee, S.; Zagorski, K.; Lyubchenko, Y.L. Supported Lipid Bilayers for Atomic Force Microscopy Studies. *Methods Mol. Biol.* **2018**, *1814*, 129–143. [[CrossRef](#)]
45. Morandat, S.; Azouzi, S.; Beauvais, E.; Mastouri, A.; El Kirat, K. Atomic Force Microscopy of Model Lipid Membranes. *Anal. Bioanal. Chem.* **2013**, *405*, 1445–1461. [[CrossRef](#)]
46. Dufrene, Y.F.; Boland, T.; Schneider, J.W.; Barger, W.R.; Lee, G.U. Characterization of the Physical Properties of Model Biomembranes at the Nanometer Scale with the Atomic Force Microscope. *Faraday Discuss.* **1999**, *111*, 79–94. [[CrossRef](#)]
47. Das, C.; Sheikh, K.H.; Olmsted, P.D.; Connell, S.D. Nanoscale Mechanical Probing of Supported Lipid Bilayers with Atomic Force Microscopy. *Phys. Rev. E* **2010**, *82*, 041920. [[CrossRef](#)]
48. Mingeot-Leclercq, M.-P.; Deleu, M.; Brasseur, R.; Dufrene, Y.F. Atomic Force Microscopy of Supported Lipid Bilayers. *Nat. Protoc.* **2008**, *3*, 1654–1659. [[CrossRef](#)]
49. Emanuele, M.; Esposito, A.; Camerini, S.; Antonucci, F.; Ferrara, S.; Seghezza, S.; Catelani, T.; Crescenzi, M.; Marotta, R.; Canale, C.; et al. Exogenous Alpha-Synuclein Alters Pre- and Post-Synaptic Activity by Fragmenting Lipid Rafts. *EBioMedicine* **2016**, *7*, 191–204. [[CrossRef](#)]
50. Canepa, P.; Canale, C.; Cavalleri, O.; Marletta, G.; Messina, G.M.L.; Messori, M.; Novelli, R.; Mattioli, S.L.; Apparente, L.; Detta, N.; et al. Adsorption of the RhNGF Protein on Polypropylene with Different Grades of Copolymerization. *Materials* **2023**, *16*, 2076. [[CrossRef](#)]
51. Morris, V.J.; Mackie, A.R.; Wilde, P.J.; Kirby, A.R.; Mills, E.C.N.; Patrick Gunning, A. Atomic Force Microscopy as a Tool for Interpreting the Rheology of Food Biopolymers at the Molecular Level. *LWT—Food Sci. Technol.* **2001**, *34*, 3–10. [[CrossRef](#)]
52. Vannozzi, L.; Gouveia, P.; Pingue, P.; Canale, C.; Ricotti, L. Novel Ultrathin Films Based on a Blend of PEG-*b*-PCL and PLLA and Doped with ZnO Nanoparticles. *ACS Appl. Mater. Interfaces* **2020**, *12*, 21398–21410. [[CrossRef](#)] [[PubMed](#)]
53. Guida, P.; Piscitelli, E.; Marrese, M.; Martino, V.; Cirillo, V.; Guarino, V.; Angeli, E.; Cocola, C.; Pelucchi, P.; Repetto, L.; et al. Integrating Microstructured Electrospun Scaffolds in an Open Microfluidic System for in Vitro Studies of Human Patient-Derived Primary Cells. *ACS Biomater. Sci. Eng.* **2020**, *6*, 3649–3663. [[CrossRef](#)] [[PubMed](#)]
54. Canepa, P.; Ghiara, G.; Spotorno, R.; Canepa, M.; Cavalleri, O. Structural vs. Electrochemical Investigation of Niobium Oxide Layers Anodically Grown in a Ca and P Containing Electrolyte. *J. Alloys Compd.* **2021**, *851*, 156937. [[CrossRef](#)]
55. Irie, Y.; Maruo, Y.; Kataoka, N.; Tanaka, H.; Kinoshita, K.; Kishida, S. AFM and XPS Study from Surfaces of Native Oxide/Al-Metal. *Procedia Eng.* **2017**, *216*, 182–189. [[CrossRef](#)]
56. Egbu, J.; Ohodnicki, J.; Paul, R.; Baltrus, J.P.; Talaat, A.; Wright, R.F.; McHenry, M.E. Analysis of Surface Roughness and Oxidation of FeNi-Based Metal Amorphous Nanocomposite Alloys. *J. Alloys Compd.* **2022**, *912*, 165155. [[CrossRef](#)]
57. Canepa, P.; Firpo, G.; Gatta, E.; Spotorno, R.; Giannoni, P.; Quarto, R.; Canepa, M.; Cavalleri, O. A Two-Step Approach to Tune the Micro and Nanoscale Morphology of Porous Niobium Oxide to Promote Osteointegration. *Materials* **2022**, *15*, 473. [[CrossRef](#)]
58. Bhatnagar, M.; Giordano, M.C.; Mennucci, C.; Chowdhury, D.; Mazzanti, A.; Valle, G.D.; Martella, C.; Tummala, P.; Lamperti, A.; Molle, A.; et al. Ultra-Broadband Photon Harvesting in Large-Area Few-Layer MoS₂ Nanostripe Gratings. *Nanoscale* **2020**, *12*, 24385–24393. [[CrossRef](#)] [[PubMed](#)]
59. Polfus, J.M.; Muñoz, M.B.; Ali, A.; Barragan-Yani, D.A.; Vullum, P.E.; Sunding, M.F.; Taniguchi, T.; Watanabe, K.; Belle, B.D. Temperature-Dependent Adhesion in van Der Waals Heterostructures. *Adv. Mater. Interfaces* **2021**, *8*, 2100838. [[CrossRef](#)]
60. Magnozzi, M.; Pflug, T.; Ferrera, M.; Pace, S.; Ramón, L.; Olbrich, M.; Canepa, P.; Ağircan, H.; Horn, A.; Forti, S.; et al. Local Optical Properties in CVD-Grown Monolayer WS₂ Flakes. *J. Phys. Chem. C* **2021**, *125*, 16059–16065. [[CrossRef](#)]
61. Zhang, H.; Huang, J.; Wang, Y.; Liu, R.; Huai, X.; Jiang, J.; Anfusio, C. Atomic Force Microscopy for Two-Dimensional Materials: A Tutorial Review. *Opt. Commun.* **2018**, *406*, 3–17. [[CrossRef](#)]
62. Sikora, A.; Woszczyzna, M.; Friedemann, M.; Ahlers, F.J.; Kalbac, M. AFM Diagnostics of Graphene-Based Quantum Hall Devices. *Micron* **2012**, *43*, 479–486. [[CrossRef](#)] [[PubMed](#)]
63. Song, J.; Zhou, Y.; Pature, N.P.; Huey, B.D. Anomalous 3D Nanoscale Photoconduction in Hybrid Perovskite Semiconductors Revealed by Tomographic Atomic Force Microscopy. *Nat. Commun.* **2020**, *11*, 3308. [[CrossRef](#)] [[PubMed](#)]
64. Buzio, R.; Calvini, P.; Ferroni, A.; Valbusa, U. Surface Analysis of Paper Documents Damaged by Foxing. *Appl. Phys. A* **2004**, *79*, 383–387. [[CrossRef](#)]

65. Huang, Z.; Stolichnov, I.; Bernard-Mantel, A.; Schott, M.; Auffret, S.; Gaudin, G.; Pizzini, S.; Ranno, L.; Setter, N. Non-Volatile Polarization Switch of Magnetic Domain Wall Velocity. *Appl. Phys. Lett.* **2015**, *107*, 252902. [[CrossRef](#)]
66. Ekar, J.; Kovač, J. AFM Study of Roughness Development during ToF-SIMS Depth Profiling of Multilayers with a Cs⁺ Ion Beam in a H₂ Atmosphere. *Langmuir* **2022**, *38*, 12871–12880. [[CrossRef](#)]
67. Buzio, R.; Toma, A.; Chincarini, A.; de Mongeot, F.B.; Boragno, C.; Valbusa, U. Atomic Force Microscopy and X-Ray Photoelectron Spectroscopy Characterization of Low-Energy Ion Sputtered Mica. *Surf. Sci.* **2007**, *601*, 2735–2739. [[CrossRef](#)]
68. Hu, C.; Li, Z. A Review on the Mechanical Properties of Cement-Based Materials Measured by Nanoindentation. *Constr. Build. Mater.* **2015**, *90*, 80–90. [[CrossRef](#)]
69. Blangiardo, A.; Lagomarsino, G.; Basso, A.; Canepa, P.; Cavalleri, O.; Rossi, S.; Monticelli, O. Preparation, Application and Recycling of a Catalytic Microflow Reactor Based on Polylactic Acid. *Appl. Surf. Sci.* **2021**, *569*, 151019. [[CrossRef](#)]
70. Bisio, F.; Palombo, M.; Prato, M.; Cavalleri, O.; Barborini, E.; Vinati, S.; Franchi, M.; Mattera, L.; Canepa, M. Optical Properties of Cluster-Assembled Nanoporous Gold Films. *Phys. Rev. B* **2009**, *80*, 205428. [[CrossRef](#)]
71. Bellotti, R.; Picotto, G.B.; Ribotta, L. AFM Measurements and Tip Characterization of Nanoparticles with Different Shapes. *Nanomanuf. Metrol.* **2022**, *5*, 127–138. [[CrossRef](#)]
72. Friedrich, S.; Cappella, B. Friction and Mechanical Properties of AFM-Scan-Induced Ripples in Polymer Films. *Front. Mech. Eng.* **2021**, *7*, 672898. [[CrossRef](#)]
73. Lin, Y.-T.; He, H.; Kaya, H.; Liu, H.; Ngo, D.; Smith, N.J.; Banerjee, J.; Borhan, A.; Kim, S.H. Photothermal Atomic Force Microscopy Coupled with Infrared Spectroscopy (AFM-IR) Analysis of High Extinction Coefficient Materials: A Case Study with Silica and Silicate Glasses. *Anal. Chem.* **2022**, *94*, 5231–5239. [[CrossRef](#)] [[PubMed](#)]
74. Chada, N.; Sigdel, K.P.; Gari, R.R.S.; Matin, T.R.; Randall, L.L.; King, G.M. Glass Is a Viable Substrate for Precision Force Microscopy of Membrane Proteins. *Sci. Rep.* **2015**, *5*, 12550. [[CrossRef](#)]
75. Kempe, A.; Schopf, J.W.; Altermann, W.; Kudryavtsev, A.B.; Heckl, W.M. Atomic Force Microscopy of Precambrian Microscopic Fossils. *Proc. Natl. Acad. Sci. USA* **2002**, *99*, 9117–9120. [[CrossRef](#)]
76. Benítez, J.J.; Guzman-Puyol, S.; Domínguez, E.; Heredia, A.; Heredia-Guerrero, J.A. Applications and Potentialities of Atomic Force Microscopy in Fossil and Extant Plant Cuticle Characterization. *Rev. Palaeobot. Palynol.* **2019**, *268*, 125–132. [[CrossRef](#)]
77. Sapienza, L.; Liu, J.; Song, J.D.; Fält, S.; Wegscheider, W.; Badolato, A.; Srinivasan, K. Combined Atomic Force Microscopy and Photoluminescence Imaging to Select Single InAs/GaAs Quantum Dots for Quantum Photonic Devices. *Sci. Rep.* **2017**, *7*, 6205. [[CrossRef](#)]
78. Hennessy, K.; Badolato, A.; Winger, M.; Gerace, D.; Atatüre, M.; Gulde, S.; Fält, S.; Hu, E.L.; Imamoglu, A. Quantum Nature of a Strongly Coupled Single Quantum Dot–Cavity System. *Nature* **2007**, *445*, 896–899. [[CrossRef](#)]
79. Müller, D.J.; Helenius, J.; Alsteens, D.; Dufrêne, Y.F. Force Probing Surfaces of Living Cells to Molecular Resolution. *Nat. Chem. Biol.* **2009**, *5*, 383–390. [[CrossRef](#)]
80. Kerdegari, S.; Canepa, P.; Odino, D.; Oropesa-Nuñez, R.; Relini, A.; Cavalleri, O.; Canale, C. Insights in Cell Biomechanics through Atomic Force Microscopy. *Materials* **2023**, *16*, 2980. [[CrossRef](#)]
81. Viljoen, A.; Mathelié-Guinlet, M.; Ray, A.; Strohmeyer, N.; Oh, Y.J.; Hinterdorfer, P.; Müller, D.J.; Alsteens, D.; Dufrêne, Y.F. Force Spectroscopy of Single Cells Using Atomic Force Microscopy. *Nat. Rev. Methods Prim.* **2021**, *1*, 63. [[CrossRef](#)]
82. Dufrêne, Y.F.; Martínez-Martín, D.; Medalsy, I.; Alsteens, D.; Müller, D.J. Multiparametric Imaging of Biological Systems by Force-Distance Curve-Based AFM. *Nat. Methods* **2013**, *10*, 847–854. [[CrossRef](#)]
83. Jalili, N.; Laxminarayana, K. A Review of Atomic Force Microscopy Imaging Systems: Application to Molecular Metrology and Biological Sciences. *Mechatronics* **2004**, *14*, 907–945. [[CrossRef](#)]
84. Lavanya, S.B.; Jayanth, G.R. Control of Interaction Force in Constant-Height Contact Mode Atomic Force Microscopy. *Mechatronics* **2022**, *88*, 102914. [[CrossRef](#)]
85. Biczysko, P.; Dzierka, A.; Józwiak, G.; Rudek, M.; Gotszalk, T.; Janus, P.; Grabiec, P.; Rangelow, I.W. Contact Atomic Force Microscopy Using Piezoresistive Cantilevers in Load Force Modulation Mode. *Ultramicroscopy* **2018**, *184*, 199–208. [[CrossRef](#)]
86. Zhong, Q.; Inniss, D.; Kjoller, K.; Elings, V.B. Fractured Polymer/Silica Fiber Surface Studied by Tapping Mode Atomic Force Microscopy. *Surf. Sci.* **1993**, *290*, L688–L692. [[CrossRef](#)]
87. Garcia, R.; Herruzo, E.T. The Emergence of Multifrequency Force Microscopy. *Nat. Nanotechnol.* **2012**, *7*, 217–226. [[CrossRef](#)]
88. Guo, S.; Solares, S.D.; Mochalin, V.; Neitzel, I.; Gogotsi, Y.; Kalinin, S.V.; Jesse, S. Multifrequency Imaging in the Intermittent Contact Mode of Atomic Force Microscopy: Beyond Phase Imaging. *Small* **2012**, *8*, 1264–1269. [[CrossRef](#)] [[PubMed](#)]
89. Dokukin, M.E.; Sokolov, I. Nanoscale Compositional Mapping of Cells, Tissues, and Polymers with Ringing Mode of Atomic Force Microscopy. *Sci. Rep.* **2017**, *7*, 11828. [[CrossRef](#)] [[PubMed](#)]
90. Zhou, X.; Fu, J.; Miao, H.; Li, F. Contact Resonance Force Microscopy with Higher-Eigenmode for Nanoscale Viscoelasticity Measurements. *J. Appl. Phys.* **2014**, *116*, 034310. [[CrossRef](#)]
91. Stan, G.; Solares, S.D.; Pittenger, B.; Erina, N.; Su, C. Nanoscale Mechanics by Tomographic Contact Resonance Atomic Force Microscopy. *Nanoscale* **2013**, *6*, 962–969. [[CrossRef](#)]
92. Radmacher, M.; Cleveland, J.P.; Fritz, M.; Hansma, H.G.; Hansma, P.K. Mapping Interaction Forces with the Atomic Force Microscope. *Biophys. J.* **1994**, *66*, 2159–2165. [[CrossRef](#)]

93. Martín-Rodríguez, A.J.; González-Orive, A.; Hernández-Creus, A.; Morales, A.; Dorta-Guerra, R.; Norte, M.; Martín, V.S.; Fernández, J.J. On the Influence of the Culture Conditions in Bacterial Antifouling Bioassays and Biofilm Properties: Shewanella Algae, a Case Study. *BMC Microbiol.* **2014**, *14*, 102. [[CrossRef](#)] [[PubMed](#)]
94. Alsteens, D.; Dupres, V.; Yunus, S.; Latgé, J.-P.; Heinisch, J.J.; Dufrêne, Y.F. High-Resolution Imaging of Chemical and Biological Sites on Living Cells Using Peak Force Tapping Atomic Force Microscopy. *Langmuir* **2012**, *28*, 16738–16744. [[CrossRef](#)]
95. Pinto, G.; Canepa, P.; Canale, C.; Canepa, M.; Cavalleri, O. Morphological and Mechanical Characterization of DNA SAMs Combining Nanolithography with AFM and Optical Methods. *Materials* **2020**, *13*, 2888. [[CrossRef](#)]
96. Chopinet, L.; Formosa, C.; Rols, M.P.; Duval, R.E.; Dague, E. Imaging Living Cells Surface and Quantifying Its Properties at High Resolution Using AFM in QI™ Mode. *Micron* **2013**, *48*, 26–33. [[CrossRef](#)] [[PubMed](#)]
97. Hansma, P.K.; Schitter, G.; Fantner, G.E.; Prater, C. High-Speed Atomic Force Microscopy. *Science* **2006**, *314*, 601–602. [[CrossRef](#)] [[PubMed](#)]
98. Viani, M.B.; Schäffer, T.E.; Palocz, G.T.; Pietrasanta, L.I.; Smith, B.L.; Thompson, J.B.; Richter, M.; Rief, M.; Gaub, H.E.; Plaxco, K.W.; et al. Fast Imaging and Fast Force Spectroscopy of Single Biopolymers with a New Atomic Force Microscope Designed for Small Cantilevers. *Rev. Sci. Instrum.* **1999**, *70*, 4300–4303. [[CrossRef](#)]
99. Humphris, A.D.L.; Miles, M.J.; Hobbs, J.K. A Mechanical Microscope: High-Speed Atomic Force Microscopy. *Appl. Phys. Lett.* **2005**, *86*, 034106. [[CrossRef](#)]
100. Sulchek, T.; Yaralioglu, G.G.; Quate, C.F.; Minne, S.C. Characterization and Optimization of Scan Speed for Tapping-Mode Atomic Force Microscopy. *Rev. Sci. Instrum.* **2002**, *73*, 2928–2936. [[CrossRef](#)]
101. Manalis, S.R.; Minne, S.C.; Quate, C.F. Atomic Force Microscopy for High Speed Imaging Using Cantilevers with an Integrated Actuator and Sensor. *Appl. Phys. Lett.* **1996**, *68*, 871–873. [[CrossRef](#)]
102. Ando, T.; Kodera, N.; Takai, E.; Maruyama, D.; Saito, K.; Toda, A. A High-Speed Atomic Force Microscope for Studying Biological Macromolecules. *Proc. Natl. Acad. Sci. USA* **2001**, *98*, 12468–12472. [[CrossRef](#)]
103. Ando, T.; Uchihashi, T.; Scheuring, S. Filming Biomolecular Processes by High-Speed Atomic Force Microscopy. *Chem. Rev.* **2014**, *114*, 3120–3188. [[CrossRef](#)] [[PubMed](#)]
104. Ando, T.; Uchihashi, T.; Fukuma, T. High-Speed Atomic Force Microscopy for Nano-Visualization of Dynamic Biomolecular Processes. *Prog. Surf. Sci.* **2008**, *83*, 337–437. [[CrossRef](#)]
105. Malkin, A.J.; Kuznetsov, Y.G.; Land, T.A.; DeYoreo, J.J.; McPherson, A. Mechanisms of Growth for Protein and Virus Crystals. *Nat. Struct. Mol. Biol.* **1995**, *2*, 956–959. [[CrossRef](#)]
106. Malkin, A.J.; Land, T.A.; Kuznetsov, Y.G.; McPherson, A.; DeYoreo, J.J. Investigation of Virus Crystal Growth Mechanisms by *In Situ* Atomic Force Microscopy. *Phys. Rev. Lett.* **1995**, *75*, 2778–2781. [[CrossRef](#)]
107. Malkin, A.J.; Kuznetsov, Y.G.; McPherson, A. Incorporation of Microcrystals by Growing Protein and Virus Crystals. *Proteins* **1996**, *24*, 247–252. [[CrossRef](#)]
108. Malkin, A.J.; Kuznetsov, Y.G.; McPherson, A. An *In Situ* AFM Investigation of Catalase Crystallization. *Surf. Sci.* **1997**, *393*, 95–107. [[CrossRef](#)]
109. Malkin, A.J.; Kuznetsov, Y.G.; Glantz, W.; McPherson, A. Atomic Force Microscopy Studies of Surface Morphology and Growth Kinetics in Thaumatin Crystallization. *J. Phys. Chem.* **1996**, *100*, 11736–11743. [[CrossRef](#)]
110. Malkin, A.J.; Kuznetsov, Y.G.; McPherson, A. Defect Structure of Macromolecular Crystals. *J. Struct. Biol.* **1996**, *117*, 124–137. [[CrossRef](#)]
111. Kuznetsov, Y.G.; Malkin, A.J.; Glantz, W.; McPherson, A. *In Situ* Atomic Force Microscopy Studies of Protein and Virus Crystal Growth Mechanisms. *J. Cryst. Growth* **1996**, *168*, 63–73. [[CrossRef](#)]
112. Konnert, J.H.; D'Antonio, P.; Ward, K.B. Observation of Growth Steps, Spiral Dislocations and Molecular Packing on the Surface of Lysozyme Crystals with the Atomic Force Microscope. *Acta Crystallogr. D* **1994**, *50*, 603–613. [[CrossRef](#)] [[PubMed](#)]
113. Yip, C.M.; Ward, M.D. Atomic Force Microscopy of Insulin Single Crystals: Direct Visualization of Molecules and Crystal Growth. *Biophys. J.* **1996**, *71*, 1071–1078. [[CrossRef](#)]
114. Land, T.A.; De Yoreo, J.J.; Lee, J.D. An *In-Situ* AFM Investigation of Canavalin Crystallization Kinetics. *Surf. Sci.* **1997**, *384*, 136–155. [[CrossRef](#)]
115. YuG, K.; Malkin, A.J.; Land, T.A.; DeYoreo, J.J.; Barba, A.P.; Konnert, J.; McPherson, A. Molecular Resolution Imaging of Macromolecular Crystals by Atomic Force Microscopy. *Biophys. J.* **1997**, *72*, 2357–2364. [[CrossRef](#)]
116. Asherie, N.; Lomakin, A.; Benedek, G.B. Phase Diagram of Colloidal Solutions. *Phys. Rev. Lett.* **1996**, *77*, 4832–4835. [[CrossRef](#)]
117. Liu, C.; Lomakin, A.; Thurston, G.M.; Hayden, D.; Pande, A.; Pande, J.; Ogun, O.; Asherie, N.; Benedek, G.B. Phase Separation in Multicomponent Aqueous-Protein Solutions. *J. Phys. Chem.* **1995**, *99*, 454–461. [[CrossRef](#)]
118. Kuznetsov, Y.G.; Konnert, J.; Malkin, A.J.; McPherson, A. The Advancement and Structure of Growth Steps on Thaumatin Crystals Visualized by Atomic Force Microscopy at Molecular Resolution. *Surf. Sci.* **1999**, *440*, 69–80. [[CrossRef](#)]
119. Malkin, A.J.; Kuznetsov, Y.G.; McPherson, A. *In Situ* Atomic Force Microscopy Studies of Surface Morphology, Growth Kinetics, Defect Structure and Dissolution in Macromolecular Crystallization. *J. Cryst. Growth* **1999**, *196*, 471–488. [[CrossRef](#)]
120. Mollica, V.; Borassi, A.; Relini, A.; Cavalleri, O.; Bolognesi, M.; Rolandi, R.; Gliozzi, A. An Atomic Force Microscopy Investigation of Protein Crystal Surface Topography. *Eur. Biophys. J.* **2001**, *30*, 313–318. [[CrossRef](#)]
121. Li, H.; Nadarajah, A.; Pusey, M.L. Determining the Molecular-Growth Mechanisms of Protein Crystal Faces by Atomic Force Microscopy. *Acta Crystallogr. D Biol. Crystallogr.* **1999**, *55*, 1036–1045. [[CrossRef](#)]

122. Durbin, S.D.; Feher, G. Studies of Crystal Growth Mechanisms of Proteins by Electron Microscopy. *J. Mol. Biol.* **1990**, *212*, 763–774. [[CrossRef](#)]
123. Malkin, A.J.; McPherson, A. Light-Scattering Investigations of Nucleation Processes and Kinetics of Crystallization in Macromolecular Systems. *Acta Crystallogr. Sect. D* **1994**, *50*, 385–395. [[CrossRef](#)]
124. Kuznetsov, Y.G.; Malkin, A.J.; Greenwood, A.; McPherson, A. Interferometric Studies of Growth Kinetics and Surface Morphology in Macromolecular Crystal Growth: Canavalin, Thaumatin, and Turnip Yellow Mosaic Virus. *J. Struct. Biol.* **1995**, *114*, 184–196. [[CrossRef](#)]
125. Larson, S.B.; Koszelak, S.; Day, J.; Greenwood, A.; Dodds, J.A.; McPherson, A. Double-Helical RNA in Satellite Tobacco Mosaic Virus. *Nature* **1993**, *361*, 179–182. [[CrossRef](#)]
126. Koszelak, S.; Day, J.; Leja, C.; Cudney, R.; McPherson, A. Protein and Virus Crystal Growth on International Microgravity Laboratory-2. *Biophys. J.* **1995**, *69*, 13–19. [[CrossRef](#)]
127. Guo, H.M.; Liu, H.W.; Wang, Y.L.; Gao, H.J.; Gong, Y.; Jiang, H.Y.; Wang, W.Q. Surface Structures of Dl-Valine and l-Alanine Crystals Observed by Atomic Force Microscopy at a Molecular Resolution. *Surf. Sci.* **2004**, *552*, 70–76. [[CrossRef](#)]
128. Wang, W.Q.; Gong, Y.; Liang, Z.; Sun, F.L.; Shi, D.X.; Gao, H.J.; Lin, X.; Jiang, P.; Wang, Z.M. Direct Observation of Surface Structure of D-Alanine and d-/l-Valine Crystals by Atomic Force Microscopy and Comparison with X-ray Diffraction Analysis. *Surf. Sci.* **2002**, *512*, L379–L384. [[CrossRef](#)]
129. Ohnishi, S.; Hara, M.; Furuno, T.; Sasabe, H. Imaging the Ordered Arrays of Water-Soluble Protein Ferritin with the Atomic Force Microscope. *Biophys. J.* **1992**, *63*, 1425–1431. [[CrossRef](#)]
130. Furuno, T.; Sasabe, H.; Ikegami, A. Imaging Two-Dimensional Arrays of Soluble Proteins by Atomic Force Microscopy in Contact Mode Using a Sharp Supertip. *Ultramicroscopy* **1998**, *70*, 125–131. [[CrossRef](#)] [[PubMed](#)]
131. Ohnishi, S.; Hara, M.; Furuno, T.; Okada, T.; Sasabe, H. Direct Visualization of Polypeptide Shell of Ferritin Molecule by Atomic Force Microscopy. *Biophys. J.* **1993**, *65*, 573–577. [[CrossRef](#)]
132. Pum, D.; Toca-Herrera, J.L.; Sleytr, U.B. S-Layer Protein Self-Assembly. *Int. J. Mol. Sci.* **2013**, *14*, 2484–2501. [[CrossRef](#)] [[PubMed](#)]
133. Houwink, A.L. A Macromolecular Mono-Layer in the Cell Wall of *Spirillum* Spec. *Biochim. Biophys. Acta* **1953**, *10*, 360–366. [[CrossRef](#)] [[PubMed](#)]
134. Messner, P.; Abdul Mazid, M.; Unger, F.M.; Sleytr, U.B. Artificial Antigens. Synthetic Carbohydrate Haptens Immobilized on Crystalline Bacterial Surface Layer Glycoproteins. *Carbohydr. Res.* **1992**, *233*, 175–184. [[CrossRef](#)] [[PubMed](#)]
135. Sleytr, U.B.; Messner, P.; Pum, D.; Sára, M. Crystalline Bacterial Cell Surface Layers (S Layers): From Supramolecular Cell Structure to Biomimetics and Nanotechnology. *Angew. Chem. Int. Ed.* **1999**, *38*, 1034–1054. [[CrossRef](#)]
136. Claus, H.; Akça, E.; Debaerdemaeker, T.; Evrard, C.; Declercq, J.-P.; Harris, J.R.; Schlott, B.; König, H. Molecular Organization of Selected Prokaryotic S-Layer Proteins. *Can. J. Microbiol.* **2005**, *51*, 731–743. [[CrossRef](#)]
137. Albers, S.-V.; Meyer, B.H. The Archaeal Cell Envelope. *Nat. Rev. Microbiol.* **2011**, *9*, 414–426. [[CrossRef](#)]
138. Hynönen, U.; Palva, A. Lactobacillus Surface Layer Proteins: Structure, Function and Applications. *Appl. Microbiol. Biotechnol.* **2013**, *97*, 5225–5243. [[CrossRef](#)]
139. Sleytr, U.B. Self-Assembly of the Hexagonally and Tetragonally Arranged Subunits of Bacterial Surface Layers and Their Reattachment to Cell Walls. *J. Ultrastruct. Res.* **1976**, *55*, 360–377. [[CrossRef](#)]
140. Sleytr, U.B.; Schuster, B.; Egelseer, E.-M.; Pum, D. S-Layers: Principles and Applications. *FEMS Microbiol. Rev.* **2014**, *38*, 823–864. [[CrossRef](#)]
141. Sleytr, U.B.; Beveridge, T.J. Bacterial S-Layers. *Trends Microbiol.* **1999**, *7*, 253–260. [[CrossRef](#)]
142. Whitman, W.B.; Coleman, D.C.; Wiebe, W.J. Prokaryotes: The Unseen Majority. *Proc. Natl. Acad. Sci. USA* **1998**, *95*, 6578–6583. [[CrossRef](#)]
143. Egelseer, E.-M.; Sára, M.; Pum, D.; Schuster, B.; Sleytr, U.B. Genetically Engineered S-Layer Proteins and S-Layer-Specific Heteropolysaccharides as Components of a Versatile Molecular Construction Kit for Applications in Nanobiotechnology. In *NanoBioTechnology: BioInspired Devices and Materials of the Future*; Shoseyov, O., Levy, I., Eds.; Humana Press: Totowa, NJ, USA, 2008; pp. 55–86; ISBN 978-1-59745-218-2.
144. Schuster, B.; Sleytr, U.B. Composite S-Layer Lipid Structures. *J. Struct. Biol.* **2009**, *168*, 207–216. [[CrossRef](#)]
145. Breitwieser, A.; Siedlaczek, P.; Lichtenegger, H.; Sleytr, U.B.; Pum, D. S-Layer Protein Coated Carbon Nanotubes. *Coatings* **2019**, *9*, 492. [[CrossRef](#)]
146. Egelseer, E.M.; Ilk, N.; Pum, D.; Messner, P.; Schäffer, C.; Schuster, B.; Sleytr, U.B. S-Layers, Microbial, Biotechnological Applications. In *Encyclopedia of Industrial Biotechnology*; John Wiley & Sons, Ltd.: Hoboken, NJ, USA, 2009; pp. 1–25; ISBN 978-0-470-05458-1.
147. Ilk, N.; Egelseer, E.M.; Sleytr, U.B. S-Layer Fusion Proteins—Construction Principles and Applications. *Curr. Opin. Biotechnol.* **2011**, *22*, 824–831. [[CrossRef](#)]
148. Schuster, B.; Pum, D.; Sára, M.; Sleytr, U.B. S-Layer Proteins as Key Components of a Versatile Molecular Construction Kit for Biomedical Nanotechnology. *Mini Rev. Med. Chem.* **2006**, *6*, 909–920. [[CrossRef](#)]
149. Schuster, B.; Sleytr, U.B. Nanotechnology with S-Layer Proteins. In *Protein Nanotechnology: Protocols, Instrumentation, and Applications*; Gerrard, J.A., Domigan, L.J., Eds.; Methods in Molecular Biology; Springer: New York, NY, USA, 2020; pp. 195–218; ISBN 978-1-4939-9869-2.

150. Damiati, S.; Peacock, M.; Mhanna, R.; Sjøpstad, S.; Sleytr, U.B.; Schuster, B. Bioinspired Detection Sensor Based on Functional Nanostructures of S-Proteins to Target the Folate Receptors in Breast Cancer Cells. *Sens. Actuators B Chem.* **2018**, *267*, 224–230. [[CrossRef](#)]
151. Schuster, B.; Sleytr, U.B. S-Layer Ultrafiltration Membranes. *Membranes* **2021**, *11*, 275. [[CrossRef](#)]
152. Schuster, B. S-Layer Protein-Based Biosensors. *Biosensors* **2018**, *8*, 40. [[CrossRef](#)]
153. Sleytr, U.B.; Glauert, A.M. Analysis of Regular Arrays of Subunits on Bacterial Surfaces; Evidence for a Dynamic Process of Assembly. *J. Ultrastruct. Res.* **1975**, *50*, 103–116. [[CrossRef](#)]
154. Sleytr, U.B.; Messner, P. Crystalline Surface Layers on Bacteria. *Annu. Rev. Microbiol.* **1983**, *37*, 311–339. [[CrossRef](#)]
155. Pavkov-Keller, T.; Howorka, S.; Keller, W. Chapter 3—The Structure of Bacterial S-Layer Proteins. In *Progress in Molecular Biology and Translational Science*; Howorka, S., Ed.; Molecular Assembly in Natural and Engineered Systems; Academic Press: Cambridge, MA, USA, 2011; Volume 103, pp. 73–130.
156. Sára, M.; Sleytr, U.B. Crystalline Bacterial Cell Surface Layers (S-Layers): From Cell Structure to Biomimetics. *Prog. Biophys. Mol. Biol.* **1996**, *65*, 83–111. [[CrossRef](#)]
157. Thornley, M.J.; Glauert, A.M.; Sleytr, U.B.; Markham, R.; Horne, R.W.; Hicks, R.M. Structure and Assembly of Bacterial Surface Layers Composed of Regular Arrays of Subunits. *Philos. Trans. R. Soc. Lond. B Biol. Sci.* **1997**, *268*, 147–153. [[CrossRef](#)]
158. Müller, D.J.; Baumeister, W.; Engel, A. Conformational Change of the Hexagonally Packed Intermediate Layer of *Deinococcus Radiodurans* Monitored by Atomic Force Microscopy. *J. Bacteriol.* **1996**, *178*, 3025–3030. [[CrossRef](#)]
159. Müller, D.J.; Baumeister, W.; Engel, A. Controlled Unzipping of a Bacterial Surface Layer with Atomic Force Microscopy. *Proc. Natl. Acad. Sci. USA* **1999**, *96*, 13170–13174. [[CrossRef](#)] [[PubMed](#)]
160. Moreno-Flores, S.; Kasry, A.; Butt, H.-J.; Vavilala, C.; Schmittel, M.; Pum, D.; Sleytr, U.B.; Toca-Herrera, J.L. From Native to Non-Native Two-Dimensional Protein Lattices through Underlying Hydrophilic/Hydrophobic Nanoprotrusions. *Angew. Chem. Int. Ed.* **2008**, *47*, 4707–4710. [[CrossRef](#)]
161. Ebner, A.; Kienberger, F.; Huber, C.; Kamruzzahan, A.S.M.; Pastushenko, V.P.; Tang, J.; Kada, G.; Gruber, H.J.; Sleytr, U.B.; Sára, M.; et al. Atomic-Force-Microscopy Imaging and Molecular-Recognition-Force Microscopy of Recrystallized Heterotetramers Comprising an S-Layer-Streptavidin Fusion Protein. *ChemBioChem* **2006**, *7*, 588–591. [[CrossRef](#)]
162. López, A.E.; Pum, D.; Sleytr, U.B.; Toca-Herrera, J.L. Influence of Surface Chemistry and Protein Concentration on the Adsorption Rate and S-Layer Crystal Formation. *Phys. Chem. Chem. Phys.* **2011**, *13*, 11905–11913. [[CrossRef](#)] [[PubMed](#)]
163. Moreno-Cencerrado, A.; Iturri, J.; Toca-Herrera, J.L. In-Situ 2D Bacterial Crystal Growth as a Function of Protein Concentration: An Atomic Force Microscopy Study. *Microsc. Res. Tech.* **2018**, *81*, 1095–1104. [[CrossRef](#)]
164. Yau, S.-T.; Vekilov, P.G. Direct Observation of Nucleus Structure and Nucleation Pathways in Apoferritin Crystallization. *J. Am. Chem. Soc.* **2001**, *123*, 1080–1089. [[CrossRef](#)]
165. Tang, J.; Krajcikova, D.; Zhu, R.; Ebner, A.; Cutting, S.; Gruber, H.J.; Barak, I.; Hinterdorfer, P. Atomic Force Microscopy Imaging and Single Molecule Recognition Force Spectroscopy of Coat Proteins on the Surface of *Bacillus Subtilis* Spore. *J. Mol. Recognit.* **2007**, *20*, 483–489. [[CrossRef](#)]
166. Chung, S.; Shin, S.-H.; Bertozzi, C.R.; De Yoreo, J.J. Self-Catalyzed Growth of S Layers via an Amorphous-to-Crystalline Transition Limited by Folding Kinetics. *Proc. Natl. Acad. Sci. USA* **2010**, *107*, 16536–16541. [[CrossRef](#)] [[PubMed](#)]
167. Richter, R.P.; Him, J.L.K.; Tessier, B.; Tessier, C.; Brisson, A.R. On the Kinetics of Adsorption and Two-Dimensional Self-Assembly of Annexin A5 on Supported Lipid Bilayers. *Biophys. J.* **2005**, *89*, 3372–3385. [[CrossRef](#)]
168. Scheuring, S.; Stahlberg, H.; Chami, M.; Houssin, C.; Rigaud, J.-L.; Engel, A. Charting and Unzipping the Surface Layer of *Corynebacterium Glutamicum* with the Atomic Force Microscope. *Mol. Microbiol.* **2002**, *44*, 675–684. [[CrossRef](#)]
169. Peyret, J.L.; Bayan, N.; Joliff, G.; Gulik-Krzywicki, T.; Mathieu, L.; Shechter, E.; Leblon, G. Characterization of the CspB Gene Encoding PS2, an Ordered Surface-Layer Protein in *Corynebacterium Glutamicum*. *Mol. Microbiol.* **1993**, *9*, 97–109. [[CrossRef](#)]
170. Bahl, H.; Scholz, H.; Bayan, N.; Chami, M.; Leblon, G.; Gulik-Krzywicki, T.; Shechter, E.; Fouet, A.; Mesnage, S.; Tosi-Couture, E.; et al. IV. Molecular Biology of S-Layers. *FEMS Microbiol. Rev.* **1997**, *20*, 47–98. [[CrossRef](#)] [[PubMed](#)]
171. Chami, M.; Bayan, N.; Peyret, J.L.; Gulik-Krzywicki, T.; Leblon, G.; Shechter, E. The S-Layer Protein of *Corynebacterium Glutamicum* Is Anchored to the Cell Wall by Its C-Terminal Hydrophobic Domain. *Mol. Microbiol.* **1997**, *23*, 483–492. [[CrossRef](#)]
172. Müller, D.J.; Fotiadis, D.; Scheuring, S.; Müller, S.A.; Engel, A. Electrostatically Balanced Subnanometer Imaging of Biological Specimens by Atomic Force Microscope. *Biophys. J.* **1999**, *76*, 1101–1111. [[CrossRef](#)] [[PubMed](#)]
173. Hoh, J.H.; Lal, R.; John, S.A.; Revel, J.-P.; Arnsdorf, M.F. Atomic Force Microscopy and Dissection of Gap Junctions. *Science* **1991**, *253*, 1405–1408. [[CrossRef](#)] [[PubMed](#)]
174. Schabert, F.A.; Henn, C.; Engel, A. Native *Escherichia Coli* OmpF Porin Surfaces Probed by Atomic Force Microscopy. *Science* **1995**, *268*, 92–94. [[CrossRef](#)]
175. Fotiadis, D.; Hasler, L.; Müller, D.J.; Stahlberg, H.; Kistler, J.; Engel, A. Surface Tongue-and-Groove Contours on Lens MIP Facilitate Cell-to-Cell Adherence. *J. Mol. Biol.* **2000**, *300*, 779–789. [[CrossRef](#)] [[PubMed](#)]
176. Shin, S.-H.; Chung, S.; Sanii, B.; Comolli, L.R.; Bertozzi, C.R.; De Yoreo, J.J. Direct Observation of Kinetic Traps Associated with Structural Transformations Leading to Multiple Pathways of S-Layer Assembly. *Proc. Natl. Acad. Sci. USA* **2012**, *109*, 12968–12973. [[CrossRef](#)] [[PubMed](#)]
177. Sleytr, U.B.; Sára, M.; Pum, D.; Schuster, B. Characterization and Use of Crystalline Bacterial Cell Surface Layers. *Prog. Surf. Sci.* **2001**, *68*, 231–278. [[CrossRef](#)]

178. Lopez, A.E.; Moreno-Flores, S.; Pum, D.; Sleytr, U.B.; Toca-Herrera, J.L. Surface Dependence of Protein Nanocrystal Formation. *Small* **2010**, *6*, 396–403. [[CrossRef](#)]
179. Györfvay, E.S.; Stein, O.; Pum, D.; Sleytr, U.B. Self-Assembly and Recrystallization of Bacterial S-Layer Proteins at Silicon Supports Imaged in Real Time by Atomic Force Microscopy. *J. Microsc.* **2003**, *212*, 300–306. [[CrossRef](#)]
180. Radmacher, M.; Fritz, M.; Hansma, P.K. Imaging Soft Samples with the Atomic Force Microscope: Gelatin in Water and Propanol. *Biophys. J.* **1995**, *69*, 264–270. [[CrossRef](#)]
181. Harrison, P.M.; Arosio, P. The Ferritins: Molecular Properties, Iron Storage Function and Cellular Regulation. *Biochim. Biophys. Acta (BBA) Bioenerg.* **1996**, *1275*, 161–203. [[CrossRef](#)]
182. Hempstead, P.D.; Yewdall, S.J.; Fernie, A.R.; Lawson, D.M.; Artymiuk, P.J.; Rice, D.W.; Ford, G.C.; Harrison, P.M. Comparison of the Three-Dimensional Structures of Recombinant Human H and Horse L Ferritins at High Resolution. Edited by R. Huber. *J. Mol. Biol.* **1997**, *268*, 424–448. [[CrossRef](#)] [[PubMed](#)]
183. Lawson, D.M.; Artymiuk, P.J.; Yewdall, S.J.; Smith, J.M.A.; Livingstone, J.C.; Treffry, A.; Luzzago, A.; Levi, S.; Arosio, P.; Cesareni, G.; et al. Solving the Structure of Human H Ferritin by Genetically Engineering Intermolecular Crystal Contacts. *Nature* **1991**, *349*, 541–544. [[CrossRef](#)]
184. Thomas, B.R.; Carter, D.; Rosenberger, F. Effect of Microheterogeneity on Horse Spleen Apoferritin Crystallization. *J. Cryst. Growth* **1998**, *187*, 499–510. [[CrossRef](#)]
185. Yau, S.-T.; Thomas, B.R.; Vekilov, P.G. Molecular Mechanisms of Crystallization and Defect Formation. *Phys. Rev. Lett.* **2000**, *85*, 353–356. [[CrossRef](#)]
186. Hurlé, D.T.J. (Ed.) *Handbook of Crystal Growth*; North-Holland: Amsterdam, The Netherlands; New York, NY, USA, 1993; ISBN 978-0-444-88908-9.
187. Morgenstern, K.; Lægsgaard, E.; Stensgaard, I.; Besenbacher, F. Transition from One-Dimensional to Two-Dimensional Island Decay on an Anisotropic Surface. *Phys. Rev. Lett.* **1999**, *83*, 1613–1616. [[CrossRef](#)]
188. Kuznetsov, Y.G.; Malkin, A.J.; McPherson, A. Atomic-Force-Microscopy Studies of Phase Separations in Macromolecular Systems. *Phys. Rev. B* **1998**, *58*, 6097–6103. [[CrossRef](#)]
189. Georgalis, Y.; Umbach, P.; Zielenkiewicz, A.; Utzig, E.; Zielenkiewicz, W.; Zielenkiewicz, P.; Saenger, W. Microcalorimetric and Small-Angle Light Scattering Studies on Nucleating Lysozyme Solutions. *J. Am. Chem. Soc.* **1997**, *119*, 11959–11965. [[CrossRef](#)]
190. Ando, T. High-Speed Atomic Force Microscopy Coming of Age. *Nanotechnology* **2012**, *23*, 062001. [[CrossRef](#)]
191. Hansma, P.K.; Cleveland, J.P.; Radmacher, M.; Walters, D.A.; Hillner, P.E.; Bezanna, M.; Fritz, M.; Vie, D.; Hansma, H.G.; Prater, C.B.; et al. Tapping Mode Atomic Force Microscopy in Liquids. *Appl. Phys. Lett.* **1994**, *64*, 1738–1740. [[CrossRef](#)]
192. Kodera, N.; Yamashita, H.; Ando, T. Active Damping of the Scanner for High-Speed Atomic Force Microscopy. *Rev. Sci. Instrum.* **2005**, *76*, 053708. [[CrossRef](#)]
193. Kokavecz, J.; Tóth, Z.; Horváth, Z.L.; Heszler, P.; Mechler, Á. Novel Amplitude and Frequency Demodulation Algorithm for a Virtual Dynamic Atomic Force Microscope. *Nanotechnology* **2006**, *17*, S173. [[CrossRef](#)]
194. Uchihashi, T.; Kodera, N.; Ando, T. Guide to Video Recording of Structure Dynamics and Dynamic Processes of Proteins by High-Speed Atomic Force Microscopy. *Nat. Protoc.* **2012**, *7*, 1193–1206. [[CrossRef](#)]
195. Uchihashi, T.; Scheuring, S. Applications of High-Speed Atomic Force Microscopy to Real-Time Visualization of Dynamic Biomolecular Processes. *Biochim. Biophys. Acta (BBA) Gen. Subj.* **2018**, *1862*, 229–240. [[CrossRef](#)]
196. Yokokawa, M.; Wada, C.; Ando, T.; Sakai, N.; Yagi, A.; Yoshimura, S.H.; Takeyasu, K. Fast-Scanning Atomic Force Microscopy Reveals the ATP/ADP-Dependent Conformational Changes of GroEL. *EMBO J.* **2006**, *25*, 4567–4576. [[CrossRef](#)]
197. Ruan, Y.; Miyagi, A.; Wang, X.; Chami, M.; Boudker, O.; Scheuring, S. Direct Visualization of Glutamate Transporter Elevator Mechanism by High-Speed AFM. *Proc. Natl. Acad. Sci. USA* **2017**, *114*, 1584–1588. [[CrossRef](#)]
198. Rangl, M.; Miyagi, A.; Kowal, J.; Stahlberg, H.; Nimigean, C.M.; Scheuring, S. Real-Time Visualization of Conformational Changes within Single MloK1 Cyclic Nucleotide-Modulated Channels. *Nat. Commun.* **2016**, *7*, 12789. [[CrossRef](#)]
199. Noi, K.; Yamamoto, D.; Nishikori, S.; Arita-Morioka, K.; Kato, T.; Ando, T.; Ogura, T. High-Speed Atomic Force Microscopic Observation of ATP-Dependent Rotation of the AAA+ Chaperone P97. *Structure* **2013**, *21*, 1992–2002. [[CrossRef](#)] [[PubMed](#)]
200. Yamashita, H.; Inoue, K.; Shibata, M.; Uchihashi, T.; Sasaki, J.; Kandori, H.; Ando, T. Role of Trimer–Trimer Interaction of Bacteriorhodopsin Studied by Optical Spectroscopy and High-Speed Atomic Force Microscopy. *J. Struct. Biol.* **2013**, *184*, 2–11. [[CrossRef](#)]
201. Shibata, M.; Yamashita, H.; Uchihashi, T.; Kandori, H.; Ando, T. High-Speed Atomic Force Microscopy Shows Dynamic Molecular Processes in Photoactivated Bacteriorhodopsin. *Nat. Nanotechnol.* **2010**, *5*, 208–212. [[CrossRef](#)] [[PubMed](#)]
202. Yokokawa, M.; Takeyasu, K. Motion of the Ca²⁺-Pump Captured. *FEBS J.* **2011**, *278*, 3025–3031. [[CrossRef](#)]
203. Heath, G.R.; Scheuring, S. Advances in High-Speed Atomic Force Microscopy (HS-AFM) Reveal Dynamics of Transmembrane Channels and Transporters. *Curr. Opin. Struct. Biol.* **2019**, *57*, 93–102. [[CrossRef](#)]
204. Sakiyama, Y.; Mazur, A.; Kapinos, L.E.; Lim, R.Y.H. Spatiotemporal Dynamics of the Nuclear Pore Complex Transport Barrier Resolved by High-Speed Atomic Force Microscopy. *Nat. Nanotechnol.* **2016**, *11*, 719–723. [[CrossRef](#)]
205. Uchihashi, T.; Iino, R.; Ando, T.; Noji, H. High-Speed Atomic Force Microscopy Reveals Rotary Catalysis of Rotorless F1-ATPase. *Science* **2011**, *333*, 755–758. [[CrossRef](#)]
206. Shibata, M.; Uchihashi, T.; Yamashita, H.; Kandori, H.; Ando, T. Structural Changes in Bacteriorhodopsin in Response to Alternate Illumination Observed by High-Speed Atomic Force Microscopy. *Angew. Chem. Int. Ed.* **2011**, *50*, 4410–4413. [[CrossRef](#)] [[PubMed](#)]

207. Eeftens, J.M.; Katan, A.J.; Kschonsak, M.; Hassler, M.; de Wilde, L.; Dief, E.M.; Haering, C.H.; Dekker, C. Condensin Smc2-Smc4 Dimers Are Flexible and Dynamic. *Cell Rep.* **2016**, *14*, 1813–1818. [[CrossRef](#)] [[PubMed](#)]
208. Shinozaki, Y.; Sumitomo, K.; Tsuda, M.; Koizumi, S.; Inoue, K.; Torimitsu, K. Direct Observation of ATP-Induced Conformational Changes in Single P2X4 Receptors. *PLoS Biol.* **2009**, *7*, e1000103. [[CrossRef](#)]
209. Igarashi, K.; Uchihashi, T.; Koivula, A.; Wada, M.; Kimura, S.; Okamoto, T.; Penttilä, M.; Ando, T.; Samejima, M. Traffic Jams Reduce Hydrolytic Efficiency of Cellulase on Cellulose Surface. *Science* **2011**, *333*, 1279–1282. [[CrossRef](#)]
210. Igarashi, K.; Koivula, A.; Wada, M.; Kimura, S.; Penttilä, M.; Samejima, M. High Speed Atomic Force Microscopy Visualizes Processive Movement of Trichoderma Reesei Cellobiohydrolase I on Crystalline Cellulose*. *J. Biol. Chem.* **2009**, *284*, 36186–36190. [[CrossRef](#)]
211. Yokokawa, M.; Yoshimura, S.H.; Naito, Y.; Ando, T.; Yagi, A.; Sakai, N.; Takeyasu, K. Fast-Scanning Atomic Force Microscopy Reveals the Molecular Mechanism of DNA Cleavage by ApaI Endonuclease. *IEE Proc. Nanobiotechnol.* **2006**, *153*, 60–66. [[CrossRef](#)] [[PubMed](#)]
212. Watanabe-Nakayama, T.; Itami, M.; Kodera, N.; Ando, T.; Konno, H. High-Speed Atomic Force Microscopy Reveals Strongly Polarized Movement of Clostridial Collagenase along Collagen Fibrils. *Sci. Rep.* **2016**, *6*, 28975. [[CrossRef](#)]
213. Crampton, N.; Yokokawa, M.; Dryden, D.T.F.; Edwardson, J.M.; Rao, D.N.; Takeyasu, K.; Yoshimura, S.H.; Henderson, R.M. Fast-Scan Atomic Force Microscopy Reveals That the Type III Restriction Enzyme EcoP15I Is Capable of DNA Translocation and Looping. *Proc. Natl. Acad. Sci. USA* **2007**, *104*, 12755–12760. [[CrossRef](#)]
214. Watanabe-Nakayama, T.; Ono, K.; Itami, M.; Takahashi, R.; Teplow, D.B.; Yamada, M. High-Speed Atomic Force Microscopy Reveals Structural Dynamics of Amyloid B1–42 Aggregates. *Proc. Natl. Acad. Sci. USA* **2016**, *113*, 5835–5840. [[CrossRef](#)]
215. Milhiet, P.-E.; Yamamoto, D.; Berthoumieu, O.; Dosset, P.; Grimellec, C.L.; Verdier, J.-M.; Marchal, S.; Ando, T. Deciphering the Structure, Growth and Assembly of Amyloid-Like Fibrils Using High-Speed Atomic Force Microscopy. *PLoS ONE* **2010**, *5*, e13240. [[CrossRef](#)]
216. Watanabe-Nakayama, T.; Sahoo, B.R.; Ramamoorthy, A.; Ono, K. High-Speed Atomic Force Microscopy Reveals the Structural Dynamics of the Amyloid- β and Amylin Aggregation Pathways. *Int. J. Mol. Sci.* **2020**, *21*, 4287. [[CrossRef](#)]
217. Endo, M.; Sugiyama, H. Single-Molecule Imaging of Dynamic Motions of Biomolecules in DNA Origami Nanostructures Using High-Speed Atomic Force Microscopy. *Acc. Chem. Res.* **2014**, *47*, 1645–1653. [[CrossRef](#)]
218. Wickham, S.F.J.; Endo, M.; Katsuda, Y.; Hidaka, K.; Bath, J.; Sugiyama, H.; Turberfield, A.J. Direct Observation of Stepwise Movement of a Synthetic Molecular Transporter. *Nat. Nanotechnol.* **2011**, *6*, 166–169. [[CrossRef](#)] [[PubMed](#)]
219. Sun, Z.; Hashemi, M.; Warren, G.; Bianco, P.R.; Lyubchenko, Y.L. Dynamics of the Interaction of RecG Protein with Stalled Replication Forks. *Biochemistry* **2018**, *57*, 1967–1976. [[CrossRef](#)] [[PubMed](#)]
220. Casuso, I.; Sens, P.; Rico, F.; Scheuring, S. Experimental Evidence for Membrane-Mediated Protein-Protein Interaction. *Biophys. J.* **2010**, *99*, L47–L49. [[CrossRef](#)] [[PubMed](#)]
221. Yamashita, H.; Voitchovsky, K.; Uchihashi, T.; Contera, S.A.; Ryan, J.F.; Ando, T. Dynamics of Bacteriorhodopsin 2D Crystal Observed by High-Speed Atomic Force Microscopy. *J. Struct. Biol.* **2009**, *167*, 153–158. [[CrossRef](#)] [[PubMed](#)]
222. Yamamoto, D.; Nagura, N.; Omote, S.; Taniguchi, M.; Ando, T. Streptavidin 2D Crystal Substrates for Visualizing Biomolecular Processes by Atomic Force Microscopy. *Biophys. J.* **2009**, *97*, 2358–2367. [[CrossRef](#)]
223. Yamamoto, D.; Ando, T. Chaperonin GroEL–GroES Functions as Both Alternating and Non-Alternating Engines. *J. Mol. Biol.* **2016**, *428*, 3090–3101. [[CrossRef](#)]
224. Ruan, Y.; Kao, K.; Lefebvre, S.; Marchesi, A.; Corringer, P.-J.; Hite, R.K.; Scheuring, S. Structural Titration of Receptor Ion Channel GLIC Gating by HS-AFM. *Proc. Natl. Acad. Sci. USA* **2018**, *115*, 10333–10338. [[CrossRef](#)]
225. Munguira, I.; Casuso, I.; Takahashi, H.; Rico, F.; Miyagi, A.; Chami, M.; Scheuring, S. Glasslike Membrane Protein Diffusion in a Crowded Membrane. *ACS Nano* **2016**, *10*, 2584–2590. [[CrossRef](#)]
226. Yilmaz, N.; Kobayashi, T. Visualization of Lipid Membrane Reorganization Induced by a Pore-Forming Toxin Using High-Speed Atomic Force Microscopy. *ACS Nano* **2015**, *9*, 7960–7967. [[CrossRef](#)]
227. Casuso, I.; Khao, J.; Chami, M.; Paul-Gilloteaux, P.; Husain, M.; Duneau, J.-P.; Stahlberg, H.; Sturgis, J.N.; Scheuring, S. Characterization of the Motion of Membrane Proteins Using High-Speed Atomic Force Microscopy. *Nat. Nanotechnol.* **2012**, *7*, 525–529. [[CrossRef](#)]
228. Colom, A.; Casuso, I.; Boudier, T.; Scheuring, S. High-Speed Atomic Force Microscopy: Cooperative Adhesion and Dynamic Equilibrium of Junctional Microdomain Membrane Proteins. *J. Mol. Biol.* **2012**, *423*, 249–256. [[CrossRef](#)] [[PubMed](#)]
229. Yilmaz, N.; Yamada, T.; Greimel, P.; Uchihashi, T.; Ando, T.; Kobayashi, T. Real-Time Visualization of Assembling of a Sphingomyelin-Specific Toxin on Planar Lipid Membranes. *Biophys. J.* **2013**, *105*, 1397–1405. [[CrossRef](#)] [[PubMed](#)]
230. Yamashita, H.; Taoka, A.; Uchihashi, T.; Asano, T.; Ando, T.; Fukumori, Y. Single-Molecule Imaging on Living Bacterial Cell Surface by High-Speed AFM. *J. Mol. Biol.* **2012**, *422*, 300–309. [[CrossRef](#)]
231. Yamamoto, D.; Uchihashi, T.; Kodera, N.; Ando, T. Anisotropic Diffusion of Point Defects in a Two-Dimensional Crystal of Streptavidin Observed by High-Speed Atomic Force Microscopy. *Nanotechnology* **2008**, *19*, 384009. [[CrossRef](#)]
232. Chiaruttini, N.; Redondo-Morata, L.; Colom, A.; Humbert, F.; Lenz, M.; Scheuring, S.; Roux, A. Relaxation of Loaded ESCRT-III Spiral Springs Drives Membrane Deformation. *Cell* **2015**, *163*, 866–879. [[CrossRef](#)] [[PubMed](#)]
233. Takahashi, H.; Miyagi, A.; Redondo-Morata, L.; Scheuring, S. Temperature-Controlled High-Speed AFM: Real-Time Observation of Ripple Phase Transitions. *Small* **2016**, *12*, 6106–6113. [[CrossRef](#)]

234. Rico, F.; Gonzalez, L.; Casuso, I.; Puig-Vidal, M.; Scheuring, S. High-Speed Force Spectroscopy Unfolds Titin at the Velocity of Molecular Dynamics Simulations. *Science* **2013**, *342*, 741–743. [[CrossRef](#)]
235. Takahashi, H.; Rico, F.; Chipot, C.; Scheuring, S. α -Helix Unwinding as Force Buffer in Spectrins. *ACS Nano* **2018**, *12*, 2719–2727. [[CrossRef](#)]
236. Rigato, A.; Miyagi, A.; Scheuring, S.; Rico, F. High-Frequency Microrheology Reveals Cytoskeleton Dynamics in Living Cells. *Nat. Phys.* **2017**, *13*, 771–775. [[CrossRef](#)] [[PubMed](#)]
237. Smolyakov, G.; Formosa-Dague, C.; Severac, C.; Duval, R.E.; Dague, E. High Speed Indentation Measures by FV, QI and QNM Introduce a New Understanding of Bionanomechanical Experiments. *Micron* **2016**, *85*, 8–14. [[CrossRef](#)]
238. Heath, G.R.; Scheuring, S. High-Speed AFM Height Spectroscopy Reveals Ms-Dynamics of Unlabeled Biomolecules. *Nat. Commun.* **2018**, *9*, 4983. [[CrossRef](#)] [[PubMed](#)]
239. Marchesi, A.; Gao, X.; Adai, R.; Rheinberger, J.; Stahlberg, H.; Nimigean, C.; Scheuring, S. An Iris Diaphragm Mechanism to Gate a Cyclic Nucleotide-Gated Ion Channel. *Nat. Commun.* **2018**, *9*, 3978. [[CrossRef](#)]
240. Morgan, J.L.W.; Evans, E.G.B.; Zagotta, W.N. Functional Characterization and Optimization of a Bacterial Cyclic Nucleotide-Gated Channel. *J. Biol. Chem.* **2019**, *294*, 7503–7515. [[CrossRef](#)] [[PubMed](#)]
241. Kaupp, U.B.; Seifert, R. Cyclic Nucleotide-Gated Ion Channels. *Physiol. Rev.* **2002**, *82*, 769–824. [[CrossRef](#)]
242. Craven, K.B.; Zagotta, W.N. CNG AND HCN CHANNELS: Two Peas, One Pod. *Annu. Rev. Physiol.* **2006**, *68*, 375–401. [[CrossRef](#)]
243. Robinson, R.B.; Siegelbaum, S.A. Hyperpolarization-Activated Cation Currents: From Molecules to Physiological Function. *Annu. Rev. Physiol.* **2003**, *65*, 453–480. [[CrossRef](#)]
244. Taylor, S.S.; Kornev, A.P. Protein Kinases: Evolution of Dynamic Regulatory Proteins. *Trends Biochem. Sci.* **2011**, *36*, 65–77. [[CrossRef](#)]
245. Eron, L.; Arditti, R.; Zubay, G.; Connaway, S.; Beckwith, J.R. An Adenosine 3':5'-Cyclic Monophosphate-Binding Protein That Acts on the Transcription Process. *Proc. Natl. Acad. Sci. USA* **1971**, *68*, 215–218. [[CrossRef](#)]
246. Pifferi, S.; Boccaccio, A.; Menini, A. Cyclic Nucleotide-Gated Ion Channels in Sensory Transduction. *FEBS Lett.* **2006**, *580*, 2853–2859. [[CrossRef](#)]
247. DiFrancesco, J.C.; DiFrancesco, D. Dysfunctional HCN Ion Channels in Neurological Diseases. *Front. Cell. Neurosci.* **2015**, *9*. [[CrossRef](#)]
248. Yu, F.H.; Yarov-Yarovoy, V.; Gutman, G.A.; Catterall, W.A. Overview of Molecular Relationships in the Voltage-Gated Ion Channel Superfamily. *Pharm. Rev.* **2005**, *57*, 387–395. [[CrossRef](#)]
249. Schmidpeter, P.A.M.; Gao, X.; Uphaday, V.; Rheinberger, J.; Nimigean, C.M. Ligand Binding and Activation Properties of the Purified Bacterial Cyclic Nucleotide-Gated Channel SthK. *J. Gen. Physiol.* **2018**, *150*, 821–834. [[CrossRef](#)]
250. Brams, M.; Kusch, J.; Spurny, R.; Benndorf, K.; Ulens, C. Family of Prokaryote Cyclic Nucleotide-Modulated Ion Channels. *Proc. Natl. Acad. Sci. USA* **2014**, *111*, 7855–7860. [[CrossRef](#)]
251. Guan, L. Structure and Mechanism of Membrane Transporters. *Sci. Rep.* **2022**, *12*, 13248. [[CrossRef](#)]
252. Zerangue, N.; Kavanaugh, M.P. Flux Coupling in a Neuronal Glutamate Transporter. *Nature* **1996**, *383*, 634–637. [[CrossRef](#)]
253. Takahashi, K.; Foster, J.B.; Lin, C.-L.G. Glutamate Transporter EAAT2: Regulation, Function, and Potential as a Therapeutic Target for Neurological and Psychiatric Disease. *Cell. Mol. Life Sci.* **2015**, *72*, 3489–3506. [[CrossRef](#)] [[PubMed](#)]
254. Tzingounis, A.V.; Wadiche, J.I. Glutamate Transporters: Confining Runaway Excitation by Shaping Synaptic Transmission. *Nat. Rev. Neurosci.* **2007**, *8*, 935–947. [[CrossRef](#)] [[PubMed](#)]
255. Danbolt, N.C. Glutamate Uptake. *Prog. Neurobiol.* **2001**, *65*, 1–105. [[CrossRef](#)] [[PubMed](#)]
256. Vandenberg, R.J.; Ryan, R.M. Mechanisms of Glutamate Transport. *Physiol. Rev.* **2013**, *93*, 1621–1657. [[CrossRef](#)]
257. Reyes, N.; Ginter, C.; Boudker, O. Transport Mechanism of a Bacterial Homologue of Glutamate Transporters. *Nature* **2009**, *462*, 880–885. [[CrossRef](#)]
258. Yernool, D.; Boudker, O.; Jin, Y.; Gouaux, E. Structure of a Glutamate Transporter Homologue from *Pyrococcus horikoshii*. *Nature* **2004**, *431*, 811–818. [[CrossRef](#)]
259. Akyuz, N.; Altman, R.B.; Blanchard, S.C.; Boudker, O. Transport Dynamics in a Glutamate Transporter Homologue. *Nature* **2013**, *502*, 114–118. [[CrossRef](#)]
260. Akyuz, N.; Georgieva, E.R.; Zhou, Z.; Stolzenberg, S.; Cuendet, M.A.; Khelashvili, G.; Altman, R.B.; Terry, D.S.; Freed, J.H.; Weinstein, H.; et al. Transport Domain Unlocking Sets the Uptake Rate of an Aspartate Transporter. *Nature* **2015**, *518*, 68–73. [[CrossRef](#)] [[PubMed](#)]
261. Erkens, G.B.; Hänel, I.; Goudsmits, J.M.H.; Slotboom, D.J.; van Oijen, A.M. Unsynchronised Subunit Motion in Single Trimeric Sodium-Coupled Aspartate Transporters. *Nature* **2013**, *502*, 119–123. [[CrossRef](#)]
262. Georgieva, E.R.; Borbat, P.P.; Ginter, C.; Freed, J.H.; Boudker, O. Conformational Ensemble of the Sodium-Coupled Aspartate Transporter. *Nat. Struct. Mol. Biol.* **2013**, *20*, 215–221. [[CrossRef](#)]
263. Hänel, I.; Wunnicke, D.; Bordignon, E.; Steinhoff, H.-J.; Slotboom, D.J. Conformational Heterogeneity of the Aspartate Transporter GltPh. *Nat. Struct. Mol. Biol.* **2013**, *20*, 210–214. [[CrossRef](#)] [[PubMed](#)]
264. Shimamoto, K.; Lebrun, B.; Yasuda-Kamatani, Y.; Sakaitani, M.; Shigeri, Y.; Yumoto, N.; Nakajima, T. DL-Threo- β -Benzyloxyaspartate, A Potent Blocker of Excitatory Amino Acid Transporters. *Mol. Pharm.* **1998**, *53*, 195–201. [[CrossRef](#)]
265. Haupts, U.; Tittor, J.; Oesterhelt, D. CLOSING IN ON BACTERIORHODOPSIN: Progress in Understanding the Molecule. *Annu. Rev. Biophys. Biomol. Struct.* **1999**, *28*, 367–399. [[CrossRef](#)]

266. Lanyi, J.K. Bacteriorhodopsin. *Annu. Rev. Physiol.* **2004**, *66*, 665–688. [[CrossRef](#)] [[PubMed](#)]
267. Kimura, Y.; Vassylyev, D.G.; Miyazawa, A.; Kidera, A.; Matsushima, M.; Mitsuoka, K.; Murata, K.; Hirai, T.; Fujiyoshi, Y. Surface of Bacteriorhodopsin Revealed by High-Resolution Electron Crystallography. *Nature* **1997**, *389*, 206–211. [[CrossRef](#)] [[PubMed](#)]
268. Luecke, H.; Schobert, B.; Richter, H.-T.; Cartailler, J.-P.; Lanyi, J.K. Structure of Bacteriorhodopsin at 1.55 Å Resolution 11 Edited by D. C. Rees. *J. Mol. Biol.* **1999**, *291*, 899–911. [[CrossRef](#)] [[PubMed](#)]
269. Zhu, R.; Canena, D.; Sikora, M.; Klausberger, M.; Seferovic, H.; Mehdipour, A.R.; Hain, L.; Laurent, E.; Monteil, V.; Wirnsberger, G.; et al. Force-Tuned Avidity of Spike Variant-ACE2 Interactions Viewed on the Single-Molecule Level. *Nat. Commun.* **2022**, *13*, 7926. [[CrossRef](#)] [[PubMed](#)]

Disclaimer/Publisher’s Note: The statements, opinions and data contained in all publications are solely those of the individual author(s) and contributor(s) and not of MDPI and/or the editor(s). MDPI and/or the editor(s) disclaim responsibility for any injury to people or property resulting from any ideas, methods, instructions or products referred to in the content.